Magnetization of Graphene with Circularly Polarized Light

by

Sina Abedi

A thesis
presented to the University of Waterloo
in fulfillment of the
thesis requirement for the degree of
Master of Applied Science
in
Electrical Engineering

Waterloo, Ontario, Canada, 2022

Author's Declaration

I hereby declare that I am the sole author of this thesis. This is a true copy of the thesis, including any required final revisions, as accepted by my examiners.

I understand that my thesis may be made electronically available to the public.

Abstract

In this thesis, the effect of circularly polarized light on a graphene sheet is explored. The fundamental question that we try to answer in this work is whether circularly polarized light is able to induce a DC magnetization in a sheet of graphene. We also consider whether that magnetization can be related to important structural constants and if the form it takes can be connected to the Inverse Faraday Effect. We first describe the basics of graphene and its lattice structure and energy dispersion. We then discuss some of the literature regarding optomagnetics and the Inverse Faraday Effect, including Pitaevskii's paper which uses the Maxwell-Abraham stress tensor to predict static magnetization in a dispersive, transparent medium. In the theoretical analysis section, we use a quantum mechanical approach to calculate modified wavefunctions for graphene using a modified Hamiltonian. After obtaining the new wavefunctions, we apply these wavefunctions in the context of a quantum mechanical expectation value to find the magnetization. We find an analytical expression for the DC magnetization which includes very important structural constants as we expected and has the form of the Inverse Faraday Effect. Finally, we present a numerical analysis which shows that DC magnetization has a maximum value and a saturation value for increasing values of the electric field amplitude E_0. We find magnetization values between $1.68 \times 10^{-13}\,\mathrm{A}$ and $3.58 \times 10^{-6}\,\mathrm{A}$ within an experimental range of applied laser intensities and wavelengths. We also find a theoretical saturation value of $1.07 \times 10^{-4}\,\mathrm{A}$ for this magnetization. Our result shows that not only can DC magnetization be induced in graphene, but within certain criteria, can be experimentally detected. This can open more possibilities for the use of graphene in the field of optomagnetics.

Acknowledgements

I would like to thank my supervisor, Prof. A. H. Majedi for his unreserved support, resourcefulness, friendliness, helpfulness, and his incredible patience with me for the past several months, in times that would subjectively be called abnormal, but nevertheless, history will say otherwise.

Dedication

This is dedicated to my parents, to whom I owe everything.

Table of Contents

List of Figures viii

1 Introduction 1

1.1 Graphene 1

1.2 Inverse Faraday Effect and Optomagnetism 5

2 Theoretical Analysis 9

2.1 Circularly Polarized Light 9

2.2 Magnetization Formula Applied to Wavefunction 25

2.3 Calculation of Expectation Value of Angular Momentum Operator 27

3 Numerical Results 34

4 Conclusion 42

References 45

APPENDICES 49

A Calculations with Linearly Polarized Light 50

B Matlab Code **57**

B.1 Integrals for the Expectation Value 57

B.2 Code for Dressed Energy Plot 58

B.3 Code for the Magnetization Plot 59

List of Figures

1.1 (a) Real-space graphene honeycomb lattice. Sublattices A and B are shown in blue and red respectively. (b) Reciprocal lattice (first Brillouin zone) with special points K, K' (also called Dirac points), M and Γ. 2

1.2 Dispersion diagram for graphene. The zoomed-in area shows the dispersion at the K point which is called the Dirac cone. 4

2.1 Diagram of the steps used in finding the dressed wavefunction of graphene. 10

2.2 Diagram of steps for finding the expression for DC magnetization of graphene. 11

2.3 Circularly polarized light applied to a sheet of graphene. 12

2.4 Gap created at the location of the Dirac cones, with a magnitude of ε_g. . . 22

2.5 Coordinate reference frame for the shifts in the orbital functions. 29

2.6 Orbital probability density for a shift in the direction of (a) $\mathbf{R}_A$, (b) $\mathbf{R}_B$. . 29

3.1 Surface plots for the dressed energy Ω with respect to field amplitude and energy, for high and low field amplitudes. Both figures are in the same frequency range of between $\omega = 1 \times 10^{15}$ s^{-1} to $\omega = 5 \times 10^{15}$ s^{-1} The electric amplitude range is (a) $E_0 = 0$ to $E_0 = 10^3$ V/m, (b) $E_0 = 10^9$ to $E_0 = 10^{10}$ V/m. 35

3.2 Surface plots for the dressed energy Ω with respect to field amplitude and energy, for high and low field amplitudes. Both figures are in the same electric field amplitude range of between $E_0 = 0$ V/m to $E_0 = 10^9$ V/m The electric amplitude range is (a) $\omega = 1 \times 10^{15}$ to $\omega = 2 \times 10^{15}$ s^{-1}, (b) $\omega = 1 \times 10^{15}$ to $\omega = 5 \times 10^{15}$ s^{-1}. 36

3.3 Magnetization plot with respect to field amplitude E_0. (a) Semi-log graph for the range of $E_0 = 10^8$ to 10^{10} V/m (intensity of 2.65×10^9 to $2.65 \times 10^{13}\,\mathrm{W/cm^2}$). (b) Log-log graph for the range of $E_0 = 10^2$ to 10^{10} V/m (intensity of 2.65×10^{-3} to $2.65 \times 10^{13}\,\mathrm{W/cm^2}$) 38

3.4 Semi-log graph of magnetization of graphene as a function of the light intensity I for the wavelength values 800nm, 1000nm, 1650nm, 2000nm and 2500nm. 39

3.5 Log-log graph of magnetization of graphene for the wavelength values 800nm, 1000nm, 1650nm, 2000nm and 2500nm within a range of field intensities $I = 10^2$ to $I = 10^{13}\,\mathrm{W/cm^2}$. Note the increased value of magnetization with increasing wavelengths for the same intensity. 40

A.1 Linearly polarized light applied to a sheet of graphene. 51

Chapter 1

Introduction

We will be looking at the effect of linearly and circularly polarized light on a sheet of graphene on the wavefunction of the graphene and analyze the effects of the the wavefunction obtained from the application of circularly polarized light on the magnetization of graphene. As such, we will first introduce the basic structure and properties of graphene, and then introduce the basic idea of the Inverse Faraday Effect and optomagnetism and how they have developed.

1.1 Graphene

Graphene is a two-dimensional sheet of carbon atoms arranged with a hexagonal or honeycomb crystal lattice which shows very special optical properties. The triangular Bravais lattice vectors are (as shown in Figure 1.1 (a)):

$$\mathbf{a}_1 = \frac{a}{2}(3, \sqrt{3}), \qquad \mathbf{a}_2 = \frac{a}{2}(3, -\sqrt{3}) \tag{1.1}$$

with $a \approx 1.42$Å being the distance between nearest-neighbour atoms.

For every elementary cell in the honeycomb lattice, there are two atoms which belong to two different sublattices, A and B. As a result, every atom from either of the two sublattices has three nearest-neighbour atoms from the other sublattice. The nearest-neighbour vectors are:

$$\boldsymbol{\delta}_1 = \frac{a}{2}(1, \sqrt{3}), \qquad \boldsymbol{\delta}_2 = \frac{a}{2}(1, -\sqrt{3}), \qquad \boldsymbol{\delta}_3 = a(-1, 0) \tag{1.2}$$

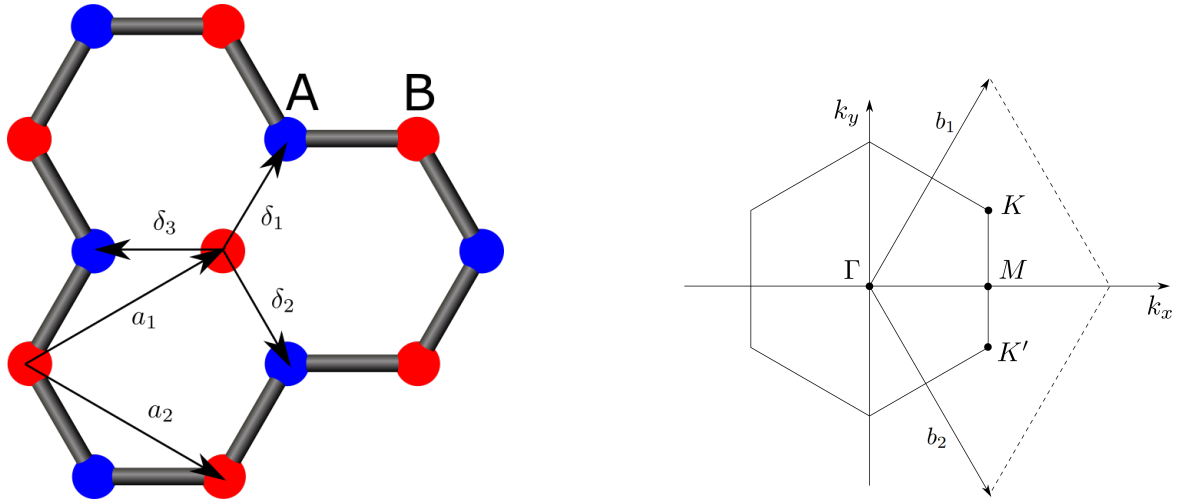

(a) (b)

Figure 1.1: (a) Real-space graphene honeycomb lattice. Sublattices A and B are shown in blue and red respectively. (b) Reciprocal lattice (first Brillouin zone) with special points K, K' (also called Dirac points), M and Γ.

The area of a primitive unit cell is

$$A_p = |\mathbf{a}_1 \times \mathbf{a}_2 \cdot \mathbf{a}_3| = \frac{3\sqrt{3}}{2}a^2 \tag{1.3}$$

where $\mathbf{a}_3 = \hat{z}$ is the unit vector pointing perpendicular to the plane of the graphene lattice [22].

The reciprocal lattice is also hexagonal with a rhomboidal unit cell. The primitive vectors for the reciprocal lattice are

$$\mathbf{b}_1 = 2\pi\frac{\mathbf{a}_2 \times \mathbf{a}_3}{\mathbf{a}_1 \times \mathbf{a}_2 \cdot \mathbf{a}_3} = \frac{4\pi}{3a}\left(\frac{1}{2}, -\frac{\sqrt{3}}{2}\right) \tag{1.4}$$

$$\mathbf{b}_2 = 2\pi\frac{\mathbf{a}_3 \times \mathbf{a}_1}{\mathbf{a}_1 \times \mathbf{a}_2 \cdot \mathbf{a}_3} = \frac{4\pi}{3a}\left(\frac{1}{2}, \frac{\sqrt{3}}{2}\right) \tag{1.5}$$

We will then have

$$\mathbf{a}_i \cdot \mathbf{b}_j = 2\pi\delta_{ij} \tag{1.6}$$

where δ_{ij} is the Kronecker delta function.

The special high symmetry points in the Brillouin zone labelled in Figure 1.1b have wave vectors

$$\mathbf{K} = \left(\frac{2\pi}{3a}, \frac{2\pi}{3\sqrt{3}a}\right), \qquad \mathbf{K}' = \left(\frac{2\pi}{3a}, -\frac{2\pi}{3\sqrt{3}a}\right), \qquad \mathbf{M} = \left(\frac{2\pi}{3a}, 0\right) \tag{1.7}$$

The electronic band structure of graphene is obtained through the tight-binding method. In this method, two Bloch functions are constructed from the atomic orbitals for the atoms in sublattice A and B. These Bloch functions which describe the π-states arising from $2p_z$ orbitals, provide the basis functions for the graphene Hamiltonian [29] (this is the starting point of our analysis in section 2.) Considering only the nearest-neighbour interactions, there is no hopping within sublattices, but rather, only between them. The tight-binding Hamiltonian can then be represented as

$$\hat{\mathcal{H}}(\mathbf{k}) = \begin{pmatrix} 0 & tS(\mathbf{k}) \\ tS^*(\mathbf{k}) & 0 \end{pmatrix} \tag{1.8}$$

where

$$S(\mathbf{k}) = \sum_{\delta} e^{i\mathbf{k}\cdot\boldsymbol{\delta}} = 2e^{\frac{ik_x a}{2}} \cos\left(\frac{k_y a\sqrt{3}}{2}\right) + e^{-ik_x a} \tag{1.9}$$

and $t \approx -2.97$ eV is the nearest-neighbour hopping parameter [14]. Defining the function $f(\mathbf{k})$ as

$$f(\mathbf{k}) = 2\cos\left(\sqrt{3}k_y a\right) + 4\cos\left(\frac{\sqrt{3}}{2}k_y a\right)\cos\left(\frac{3}{2}k_x a\right) \tag{1.10}$$

the energy can be written as

$$E(\mathbf{k}) = \pm t|S(\mathbf{k})| = \pm t\sqrt{3 + f(\mathbf{k})} \tag{1.11}$$

The energy dispersion diagram resulting from Eq (1.11) is shown in Figure 1.2. As can be seen, the energy dispersion around these points is conical without any gaps between the valence band and the conduction band. As such, graphene is called a gapless semiconductor [14] and can also be called a semimetal as shown in the work of Burkov, A. [5]. A main part of our analysis will include the opening of this gap through the application of circularly polarized light to the graphene sheet.

The effective Hamiltonian near the symmetry points K and K' is

$$\hat{\mathcal{H}}_{K,K'}(\mathbf{q}) = \hbar v \begin{pmatrix} 0 & q_x \mp iq_y \\ q_x \pm iq_y & 0 \end{pmatrix} \tag{1.12}$$

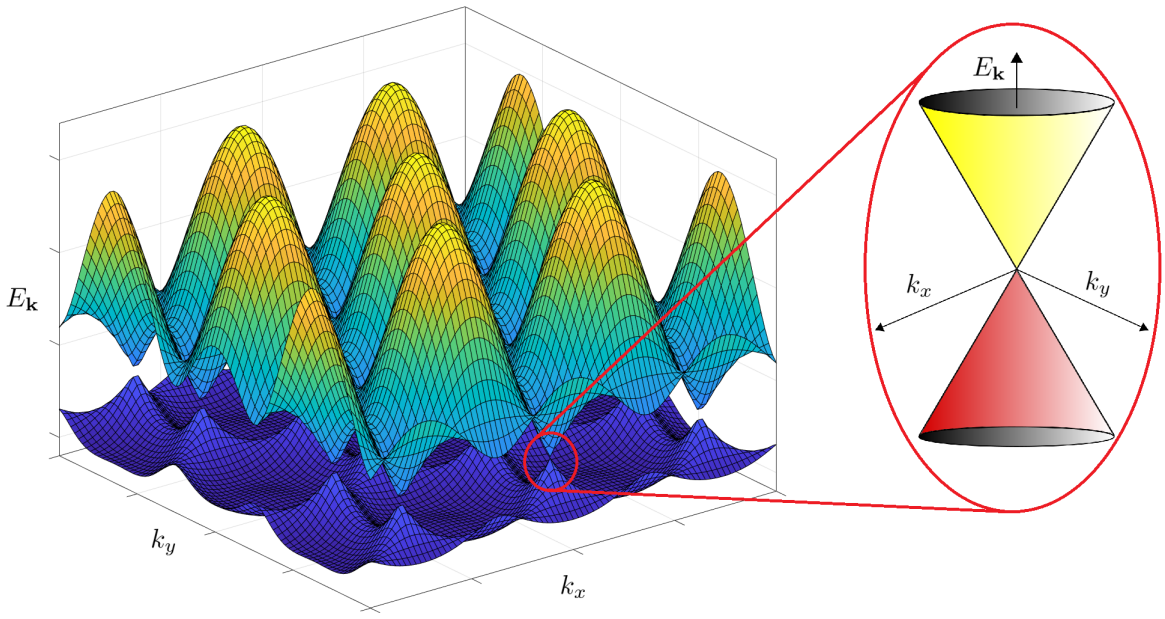

Figure 1.2: Dispersion diagram for graphene. The zoomed-in area shows the dispersion at the K point which is called the Dirac cone.

where $v = \dfrac{3a|t|}{2\hbar}$ is the electron velocity at the Dirac cones [14]. In the vicinity of the Dirac points, this velocity is approximately equal to 1.0×10^6m/s. Oftentimes in literature, the Hamiltonian in Eq (1.12) is also written as [22] [14]:

$$\hat{\mathcal{H}}_K = v\boldsymbol{\sigma} \cdot \hbar\mathbf{k} \tag{1.13}$$

where $\boldsymbol{\sigma} = (\sigma_x, \sigma_y)$ is the Pauli matrix vector:

$$\sigma_x = \begin{pmatrix} 0 & 1 \\ 1 & 0 \end{pmatrix}, \qquad \sigma_y = \begin{pmatrix} 0 & -i \\ i & 0 \end{pmatrix} \tag{1.14}$$

This is an equivalent form of Eq (1.12) where instead of $\mathbf{q}$, $\mathbf{k}$ is taken to be the wave vector and the Hamiltonian is only considered around the K point, instead of both the K and K' points. We will use the form of the Hamiltonian from Eq (1.13) for our calculations in the theoretical analysis section.

1.2 Inverse Faraday Effect and Optomagnetism

Optomagnetism originally comes from nonlinear interactions between the spin and orbital magnetic moments of electronic structures with intensive not-linearly polarized light (e.g. circularly polarized light) where the control, generation and detection of magnetization in materials is determined by the gyration or angular momentum of light. The optomagnetic effect is mostly researched in terms of the IFE (Inverse Faraday Effect), and that will be the central result of the thesis.

It is difficult to come up with an exact point of beginning for the field of optomagnetism, but the best point of departure for our current purposes is the paper that laid the theoretical foundations for the IFE. In his paper in 1960, L. P. Pitaevskii uses a phenomenological approach using the Maxwell-Abraham stress tensor to predict static magnetization in a dispersive and transparent medium. Subsequently in 1965, van der Ziel *et al.* [34] observed this effect experimentally and coined the term Inverse Faraday Effect. They derived an expression for the static magnetization using a potential function [25] and derived the expression for magnetization in the form

$$M = -\frac{\partial F}{\partial \mathbf{H}} = -\gamma \left(\mathcal{E}_R \mathcal{E}_R^* - \mathcal{E}_L \mathcal{E}_L^* \right), \tag{1.15}$$

where F is the potential function, $\mathbf{H}$ is the DC magnetic field, γ is the optical gyration coefficient and $\mathcal{E}_R$ and $\mathcal{E}_L$ are the amplitudes of the right and left circularly polarized light respectively. This relation is also written as

$$M(t) = -\gamma \mathbf{E}^*(t) \times \mathbf{E}(t). \tag{1.16}$$

This equation connects the magnetization to the generating electric field of the light pulse. They also showed that the generated magnetic moment was proportional to the Verdet constant of the material, demonstrating the connection between the Faraday effect and the IFE (See also Shen (2002) [30, Chapter 5]).

Furthermore, Pershan *et al.* [26] provided a detailed quantum-mechanical explanation of the IFE by formulating an effective Hamiltonian for the process and linearizing the nonlinear problem through it. For example, for a spin-$\frac{1}{2}$ system, the effective Hamiltonian is given as $\mathcal{H}_{\text{eff}} = iA\mathbf{S}\cdot\mathcal{E}\times\mathcal{E}^*$ with $\mathbf{S}$ as the spin matrix and A as a phenomenological constant. It is important to note that the IFE is a nonlinear optical effect creating nonequilibrium magnetization without scattering of light. This implies that after interaction with spins, the spectral distribution of light does not change and only the average number of photons decreases, reflecting the energy transfer between the spin system and light [9].

To see the nonlinearity of this optical effect clearly, we look at the dynamics and interaction of magnetic moments with magnetic fields through the Landau-Lifshitz equation. For a volume V of a magnetized solid, the magnetic moment is given by $\mathbf{m} = V\mathbf{M}$ where $\mathbf{M}$ is the magnetization and $\mathbf{m}$ is the magnetic moment of a given volume. All interactions contribute to a thermodynamical potential $\mathbf{\Phi}$ and the action of these combined can be considered as the effective magnetic field

$$\mathbf{H}^{\text{eff}} = -\frac{\partial \mathbf{\Phi}}{\partial \mathbf{M}}. \tag{1.17}$$

The Landau-Lifshitz equation corresponds to the motion of the magnetization vector [21]:

$$\frac{d\mathbf{m}}{dt} = \gamma \mathbf{m} \times \mathbf{H}^{\text{eff}}, \tag{1.18}$$

describing the magnetic moment precession around the effective magnetic field. The full expression for the thermodynamical potential (neglecting terms with orders higher than 3 in $\mathbf{E}(\omega)$) can be written as

$$\begin{aligned} \mathbf{\Phi} = {} & \chi^{(l)}_{ij} E_i(\omega)^* E_j(\omega) + \alpha^{(l)}_{ijk} E_i(\omega)^* E_j(\omega) M_k(0) \\ & + \beta^{(l)}_{ijk} E_i(\omega)^* E_j(\omega) l_k(0) + \chi^{(nl)}_{ijk} E_i(2\omega)^* E_j(\omega) E_k(\omega) \\ & + \alpha^{(nl)}_{ijkl} E_i(2\omega)^* E_j(\omega) E_k(\omega) M_l(0) + \beta^{(nl)}_{ijkl} E_i(2\omega)^* E_j(\omega) E_k(\omega) l_l(0) \end{aligned} \tag{1.19}$$

where $\chi^{(l)}_{ij}$, $\chi^{(nl)}_{ijk}$, $\alpha^{(l)}_{ijk}$, $\alpha^{(nl)}_{ijkl}$, $\beta^{(l)}_{ijk}$, $\beta^{(nl)}_{ijkl}$ are tensors that describe the optical properties of the material and the superscript l corresponds to the linear response, and the superscript nl corresponds to the nonlinear response and $\mathbf{M}(0)$ and $\mathbf{l}(0)$ correspond to the static magnetization and the antiferromagnetic vector respectively [25]. The Faraday Effect and the Inverse Faraday Effect were derived from equation (1.19). The Faraday Effect involves the rotation of linearly polarized light passing through a material under a magnetic field, while the IFE is the process of circularly polarized light creating a magnetization in a material. As such, the strength and degree of rotation (measured by the Verdet constant) that the linearly polarized light undergoes in the Faraday Effect is also a measure and determining factor of the strength of the IFE and the resulting static magnetization.

With the discovery of ultrafast demagnetization of a Ni film by 60 fs optical laser pulse by Beaurepaire *et al.* (1996) [2], a new field of ultrafast manipulation of magnetization was created. After this paper, there were many experiments aimed at demonstrating other possibilities such as laser-induced spin orientation [15] and optical generation of coherent magnetic precession [12] on time scales of 1 ps or less. In general, there are three classes describing the effects of pump laser pulses on magnetic systems [17]:

1. Thermal effects are caused by absorption of photons as energy is pumped into the material. The magnetization change is thus an effect of the spin temperature $M = M(T_s)$. Phonons and electrons are pumped with the energy from light. Any subsequent magnetization changes and their time scales are determined by the internal equilibration processes like electron-spin interactions, which can be as low as 50 fs for ferromagnets. External parameters such as thermal conductivity of substrates and the geometry of the material give the lifetime of such thermal effects. This class is limited by the cooling time as it limits the repetition frequency of the magnetization manipulation through spin excitation.

2. Nonthermal photomagnetic effects involve the absorption of pump photons [13]. For this class, through certain electronic states that have direct influence on magnetic parameters such as magnetocrystalline anisotropy, photons are absorbed. Through these same magnetic parameters, the magnetic moment of the material is affected and the lifetime of the effect is given by the lifetime of the corresponding electronic states.

3. Nonthermal optomagnetic effects are unrelated to the absorption of pump photons and are seen mostly in transparent crystals [13]. They are based on an optically coherent stimulated Raman scattering mechanism and mainly include effects such as the IFE and the Inverse Cotton-Mouton effect. This mechanism's action can be considered as instantaneous and the spin-orbit coupling which is the driving force for the magnetization change is its limiting factor. The lifetime of the effect is similar to optical coherence (100–200 fs).

The publication by Kimel *et al.* [16] had managed to experimentally demonstrate for the first time, that spins can be manipulated with a circularly polarized laser beam [10]. This was a major milestone in the understanding of optomagnetism. Not only had it managed to demonstrate this effect, it utilized this effect for ultrafast non-thermal coherent control of magnetization and spin dynamics in magnets through the application of these circularly polarized femtosecond light pulses with the use of the IFE. Until then, IFE had remained relatively unknown and unexplored experimentally, and only in a limited form was the basic theory of the process theoretically explored. There were papers which focused on thermal and photomagnetic effects. For example, Kimel *et al.* (2004) [15] had already shown a laser-induced ultrafast spin reorientation in TmFeO3 on a timescale of a few picoseconds, contrasting to what was previously hundreds of picoseconds. Photomagnetic effects were already shown to exist in garnets with certain dopants [32] and Duong *et al.* (2004) [7] had probed and examined magnetic changes that were caused by the photoexcitation of NiO by optical second-harmonic generation.

The paper by Kimel *et al.* [16] starts from the basic theory of the IFE, with the equation for Faraday rotation through a medium under a magnetic field:

$$\alpha_F = \frac{\chi}{n}\mathbf{M}\cdot\mathbf{k} \tag{1.20}$$

where n is the refractive index of the material, $\mathbf{k}$ is the wave vector of light and $\mathbf{M}$ is the magnetization. They use the expression for the magnetization from the basic theory for IFE:

$$\mathbf{M}(0) = \frac{\chi}{16\pi}\left[\mathbf{E}(\omega)\times\mathbf{E}^*(\omega)\right] \tag{1.21}$$

where χ is the magnetic susceptibility. This is another form of the equations we have previously shown. They used DyFeO3 for their experiment as it had a strong anisotropy of the magnetic susceptibility χ. Finally, they were able to show that an ultrashort laser pulse will act on the ensemble of strongly correlated spins, acting as a magnetic field pulse which is directed along the wave vector $\mathbf{k}$. They showed that such femtosecond circularly polarized laser pulses are equivalent to 200 fs magnetic pulses up to 5T [16].

Consequently, new research was beginning to find more applications for the IFE and optomagnetic effects. Hertel (2005) explored the theoretical side of the IFE in metals using a microscopic approach based on the Drude approximation of a free-electron gas, where the magnetization due to IFE was interpreted as a result of microscopic solenoidal currents generated by electromagnetic waves [10]. It was shown by Stanciu, Hansteen, *et al.* (2007) [31] that IFE could be used to reverse magnetization in a controllable way with a single 40 fs circularly polarized laser pulse without the use of any applied magnetic field. Others such as Popova *et al.* (2011) [27] have tried to correct some of the shortcomings of the theory behind IFE to account for extremely short laser pulse durations which cause problems for the original formulation. Others such as Battiato *et al.* (2014) [1] further explored the quantum mechanical model of the IFE using perturbations in conjunction with an analytical time-dependent solution of the Liouville-von Neumann equation and the density matrix approach. The interest in optical control of magnetization and specifically the IFE has consistently increased and can be seen by the papers from Lambert *et al.* (2014) [20] and Kozhaev *et al.* [18]. Tokman *et al.* [33] published a paper on the IFE effect in graphene which attempts to address the same issue as we do in this thesis, with a completely different approach. We will compare our results with those of Tokman *et al.* in the next chapters. More recently, Majedi, A. Hamed and Lounis, Brahim [23] developed a quantum mechanical formulation for a generalized Pitaevskii's relationship and showed that photoinduced DC magnetization is proportional to the odd harmonics of light power. Our purpose here is to apply a similar methodology with graphene and theoretically determine whether we can induce DC magnetization in graphene, and whether this magnetization follows the same form as the IFE observed in previous research.

Chapter 2

Theoretical Analysis

2.1 Circularly Polarized Light

Before we begin with the calculations, we will give a summary of the method and the steps used to obtain the final result. We first start from the Hamiltonian of graphene around the K point, which includes the interaction term coming from the vector potential of the circularly polarized light that we apply to the graphene. This will break up our total Hamiltonian into two parts: 1) $\hat{\mathcal{H}}_k$ which is the original Hamiltonian and 2) $\hat{\mathcal{H}}_0$ which is the interaction Hamiltonian.

We then solve Schrödinger's equation for the interaction Hamiltonian and obtain the wavefunctions which we name $\psi_0^{\pm}$. In order to solve for the wavefunction considering the total Hamiltonian, we assume the form of the solution $\psi_{\mathbf{k}}$ is a combination of functions of time $\xi^{\pm}(t)$ multiplied by the interaction wavefunctions found in the previous step. We then plug our assumptions into Schrödinger's equation with the full Hamiltonian to arrive at a system of ODEs. This system turns out to have non-constant coefficients, so we use an approximation to simplify it to a system with constant coefficients. We then solve this system and arrive at the total wavefunction $\psi_{\mathbf{k}}$ for both the conduction and valence band.

After finding the total wavefunction, we use the formula from the paper by Majedi, A. Hamed and Lounis, Brahim [23] for magnetization, which involves taking the expectation value of the total angular momentum operator. Since our basis functions are orbital functions, we break up the angular momentum operator into two parts, one for $\mathbf{r} \times \mathbf{p}$ and one for $\mathbf{r} \times e\mathbf{A}$. We then apply translations to the two orbital functions for the A and B atom to account for their physical translation in space. After showing that the expectation values

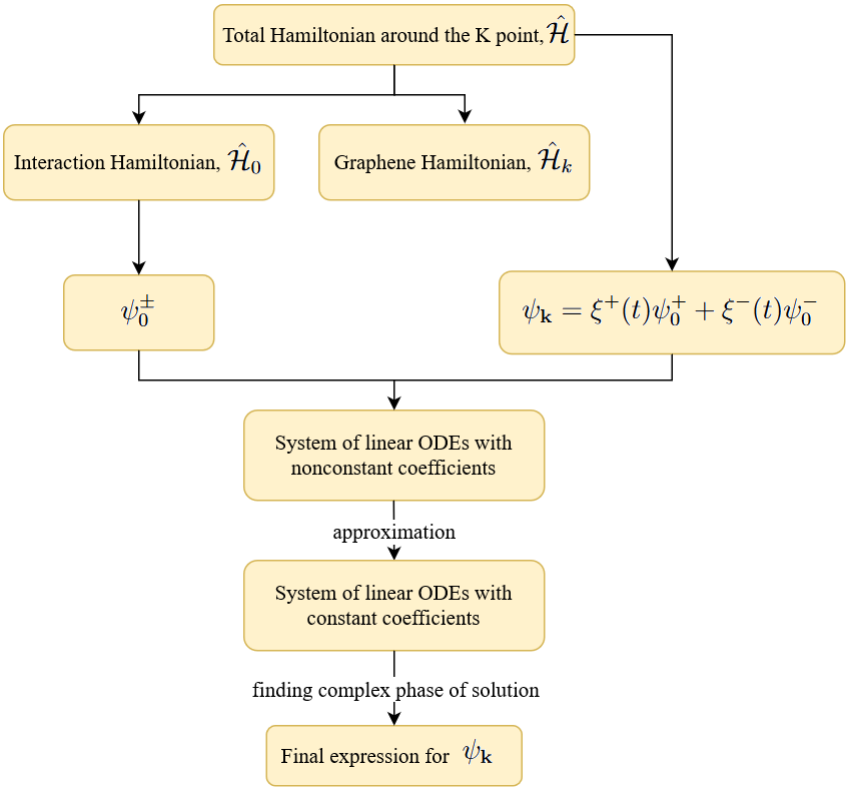

Figure 2.1: Diagram of the steps used in finding the dressed wavefunction of graphene.

for the first part of the angular momentum operator is zero, we use Matlab to numerically solve the integrals arising from the expectation values of the second part of that operator.

Finally, after obtaining the values for these integrals, we combine the integrals with the constant terms that we obtain from the multiplication $\psi_{\mathbf{k}}^*\psi_{\mathbf{k}}$ and show the complete expression for the magnetization of graphene (refer to Figures 2.1 and 2.2 for a visual representation of the steps.)

For graphene, the Hamiltonian in the presence of an electromagnetic field can be written in the following form:

$$\hat{\mathcal{H}} = v\boldsymbol{\sigma} \cdot (\hbar\mathbf{k} - e\mathbf{A}) \tag{2.1}$$

where $\mathbf{A} = (A_x, A_y)$ is the magnetic vector potential, $\boldsymbol{\sigma} = (\sigma_x, \sigma_y)$ is the Pauli matrix vector and $\mathbf{k} = (k_x, k_y) = (k\cos\varphi, k\sin\varphi)$ is the wave vector and φ is the azimuth angle of the electron wave vector. To find the dressed states in graphene, we follow a similar

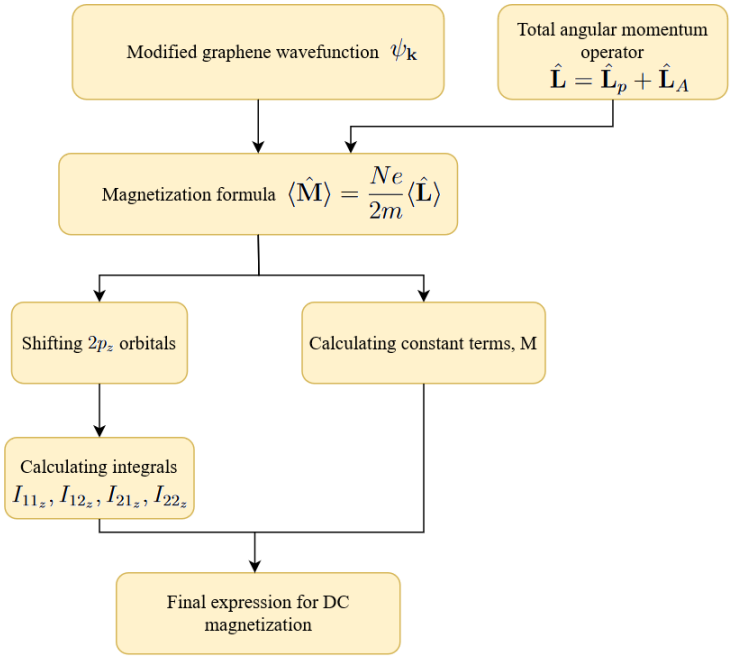

Figure 2.2: Diagram of steps for finding the expression for DC magnetization of graphene.

methodology as the one used in the paper by Kristinsson, K., Kibis, O., Morina, S. and I. A. Shelykh [19], by applying a circularly polarized field to the graphene and solve the corresponding Schrödinger's equation using the above Hamiltonian, as illustrated in Figure 2.3. Since we are using circularly polarized light, our vector potential will have the following form:

$$\mathbf{A} = (A_0 \cos \omega t, A_0 \sin \omega t) \tag{2.2}$$

where

$$A_0 = \frac{E_0}{\omega} \tag{2.3}$$

We will have two parts to our Hamiltonian if we expand the total Hamiltonian

$$\hat{\mathcal{H}} = \hat{\mathcal{H}}_0 + \hat{\mathcal{H}}_k \tag{2.4}$$

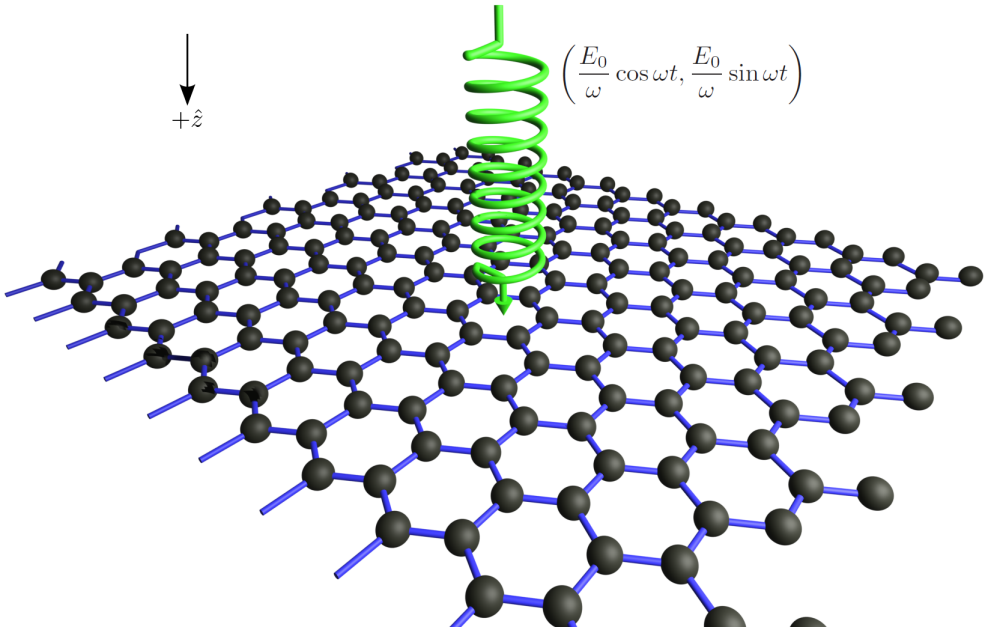

Figure 2.3: Circularly polarized light applied to a sheet of graphene.

First we find the interaction Hamiltonian $\hat{\mathcal{H}}_0$:

$$\begin{aligned}
\hat{\mathcal{H}}_0 &= -v\boldsymbol{\sigma}\cdot e\mathbf{A} \\
&= -ve(\sigma_x A_x + \sigma_y A_y) \\
&= -ve\left[\begin{pmatrix}0 & 1\\ 1 & 0\end{pmatrix}(A_0\cos\omega t) + \begin{pmatrix}0 & -i\\ i & 0\end{pmatrix}(A_0\sin\omega t)\right] \\
&= (-veA_0)\begin{pmatrix}0 & \cos\omega t - i\sin\omega t\\ \cos\omega t + i\sin\omega t & 0\end{pmatrix} \\
\hat{\mathcal{H}}_0 &= (-veA_0)\begin{pmatrix}0 & e^{i\omega t}\\ e^{-i\omega t} & 0\end{pmatrix} \qquad (2.5)
\end{aligned}$$

Next we find the graphene Hamiltonian $\hat{\mathcal{H}}_k$:

$$\begin{aligned}
\hat{\mathcal{H}}_k &= v\boldsymbol{\sigma}\cdot\hbar\mathbf{k} \\
&= v\hbar(\sigma_x k_x + \sigma_y k_y) \\
&= v\hbar\left[\begin{pmatrix}0 & 1\\ 1 & 0\end{pmatrix}k_x + \begin{pmatrix}0 & -i\\ i & 0\end{pmatrix}k_y\right] \\
&= v\hbar\begin{pmatrix}0 & k_x - ik_y\\ k_x + ik_y & 0\end{pmatrix} \\
\hat{\mathcal{H}}_k &= \begin{pmatrix}0 & v\hbar(k_x - ik_y)\\ v\hbar(k_x + ik_y) & 0\end{pmatrix}
\end{aligned} \tag{2.6}$$

We arrive at the following wavefunctions that are also derived by Kristinsson *et al.* [19] by solving the system of equations $i\hbar\frac{d}{dt}\psi_0 = \hat{\mathcal{H}}_0\psi_0$:

$$\psi_0^{\pm} = e^{\pm\frac{i\Omega t}{2\hbar}}\left[\sqrt{\frac{\Omega \pm \hbar\omega}{2\Omega}}\Phi_1'(\mathbf{r})e^{-\frac{i\omega t}{2}} \pm \sqrt{\frac{\Omega \mp \hbar\omega}{2\Omega}}\Phi_2'(\mathbf{r})e^{\frac{i\omega t}{2}}\right] \tag{2.7}$$

where we define the new energy of the system dressed by circularly polarized light as

$$\Omega = \sqrt{(\hbar\omega)^2 + \left(\frac{2veE_0}{\omega}\right)^2} \tag{2.8}$$

We can see from equation (2.8) that the frequency of the system is also being dressed. Taking $\Omega = \hbar\omega_{\text{dressed}}$, we get the expression for the dressed frequency, $\omega_{\text{dressed}} = \sqrt{\omega^2 + \left(\frac{2veE_0}{\hbar\omega}\right)^2}$. We put these wavefunctions in vector form, using $\Phi_1'(\mathbf{r})$ and $\Phi_2'(\mathbf{r})$ as the basis vectors

$$\begin{aligned}
\psi_0^+ &= \begin{pmatrix}\psi_{01}^+\\ \psi_{02}^+\end{pmatrix} = \begin{pmatrix}\sqrt{\frac{\Omega+\hbar\omega}{2\Omega}}e^{\frac{i\Omega t}{2\hbar}-\frac{i\omega t}{2}}\\ \sqrt{\frac{\Omega-\hbar\omega}{2\Omega}}e^{\frac{i\Omega t}{2\hbar}+\frac{i\omega t}{2}}\end{pmatrix} \\
\psi_0^- &= \begin{pmatrix}\psi_{01}^-\\ \psi_{02}^-\end{pmatrix} = \begin{pmatrix}\sqrt{\frac{\Omega-\hbar\omega}{2\Omega}}e^{-\frac{i\Omega t}{2\hbar}-\frac{i\omega t}{2}}\\ -\sqrt{\frac{\Omega+\hbar\omega}{2\Omega}}e^{-\frac{i\Omega t}{2\hbar}+\frac{i\omega t}{2}}\end{pmatrix} \\
\dot{\psi}_0^+ &= \begin{pmatrix}\dot{\psi}_{01}^+\\ \dot{\psi}_{02}^+\end{pmatrix} = \begin{pmatrix}i\left(\frac{\Omega-\hbar\omega}{2\hbar}\right)\sqrt{\frac{\Omega+\hbar\omega}{2\Omega}}e^{\frac{i\Omega t}{2\hbar}-\frac{i\omega t}{2}}\\ i\left(\frac{\Omega+\hbar\omega}{2\hbar}\right)\sqrt{\frac{\Omega-\hbar\omega}{2\Omega}}e^{\frac{i\Omega t}{2\hbar}+\frac{i\omega t}{2}}\end{pmatrix} \\
\dot{\psi}_0^- &= \begin{pmatrix}\dot{\psi}_{01}^-\\ \dot{\psi}_{02}^-\end{pmatrix} = \begin{pmatrix}-i\left(\frac{\Omega+\hbar\omega}{2\hbar}\right)\sqrt{\frac{\Omega-\hbar\omega}{2\Omega}}e^{-\frac{i\Omega t}{2\hbar}-\frac{i\omega t}{2}}\\ i\left(\frac{\Omega-\hbar\omega}{2\hbar}\right)\sqrt{\frac{\Omega+\hbar\omega}{2\Omega}}e^{-\frac{i\Omega t}{2\hbar}+\frac{i\omega t}{2}}\end{pmatrix}
\end{aligned} \tag{2.9}$$

$\psi_{\mathbf{k}}$ will have the following form

$$\psi_{\mathbf{k}} = \xi^+(t)\psi_0^+ + \xi^-(t)\psi_0^- \tag{2.10}$$

$$= \xi^+(t)\begin{pmatrix}\psi_{01}^+\\ \psi_{02}^+\end{pmatrix} + \xi^-(t)\begin{pmatrix}\psi_{01}^-\\ \psi_{02}^-\end{pmatrix} \tag{2.11}$$

$$\begin{pmatrix}\psi_{\mathbf{k}_1}\\ \psi_{\mathbf{k}_2}\end{pmatrix} = \begin{pmatrix}\xi^+(t)\psi_{01}^+ + \xi^-(t)\psi_{01}^-\\ \xi^+(t)\psi_{02}^+ + \xi^-(t)\psi_{02}^-\end{pmatrix} \tag{2.12}$$

We have the Hamiltonian

$$\hat{\mathcal{H}} = \begin{pmatrix}0 & -\frac{W_0}{2}e^{-i\omega t} + \hbar v(k_x - ik_y)\\ -\frac{W_0}{2}e^{i\omega t} + \hbar v(k_x + ik_y) & 0\end{pmatrix} \tag{2.13}$$

$$\hat{\mathcal{H}} = \begin{pmatrix}0 & H_1\\ H_2 & 0\end{pmatrix} \tag{2.14}$$

where

$$W_0 = 2veA_0 \tag{2.15}$$

The Schrödinger equation has the following form

$$i\hbar\dot{\psi}_{\mathbf{k}} = \hat{\mathcal{H}}\psi_{\mathbf{k}} \tag{2.16}$$

Applying the product rule to the derivative of $\psi_{\mathbf{k}}$

$$\dot{\psi}_{\mathbf{k}} = \dot{\xi}^+(t)\psi_0^+ + \xi^+(t)\dot{\psi}_0^+ + \dot{\xi}^-(t)\psi_0^- + \xi^-(t)\dot{\psi}_0^- \tag{2.17}$$

On the right hand side of equation (2.16), we have

$$\hat{\mathcal{H}}\psi_{\mathbf{k}} = \begin{pmatrix}0 & H_1\\ H_2 & 0\end{pmatrix}\begin{pmatrix}\psi_{\mathbf{k}_1}\\ \psi_{\mathbf{k}_2}\end{pmatrix} = \begin{pmatrix}H_1\psi_{\mathbf{k}_2}\\ H_2\psi_{\mathbf{k}_1}\end{pmatrix} \tag{2.18}$$

The full Schrödinger equation will now be the following

$$i\hbar\left[\dot{\xi}^+\begin{pmatrix}\psi_{01}^+\\ \psi_{02}^+\end{pmatrix} + \xi^+\begin{pmatrix}\dot{\psi}_{01}^+\\ \dot{\psi}_{02}^+\end{pmatrix} + \dot{\xi}^-\begin{pmatrix}\psi_{01}^-\\ \psi_{02}^-\end{pmatrix} + \xi^-\begin{pmatrix}\dot{\psi}_{01}^-\\ \dot{\psi}_{02}^-\end{pmatrix}\right] = \begin{pmatrix}H_1\psi_{\mathbf{k}_2}\\ H_2\psi_{\mathbf{k}_1}\end{pmatrix} \tag{2.19}$$

This leads to two sets of coupled differential equations

$$i\hbar\left[\dot{\xi}^+\psi_{01}^+ + \xi^+\dot{\psi}_{01}^+ + \dot{\xi}^-\psi_{01}^- + \xi^-\dot{\psi}_{01}^-\right] = H_1\psi_{\mathbf{k}_2} \tag{2.20}$$

$$i\hbar\left[\dot{\xi}^+\psi_{02}^+ + \xi^+\dot{\psi}_{02}^+ + \dot{\xi}^-\psi_{02}^- + \xi^-\dot{\psi}_{02}^-\right] = H_2\psi_{\mathbf{k}_1} \tag{2.21}$$

Rearranging equation (2.21) in terms of $\dot{\xi}^-$:

$$\dot{\xi}^- = \frac{H_2\psi_{\mathbf{k}_1} - i\hbar\left[\dot{\xi}^+\psi_{02}^+ + \xi^+\dot{\psi}_{02}^+ + \xi^-\dot{\psi}_{02}^-\right]}{i\hbar\psi_{02}^-} \tag{2.22}$$

Subbing in equation (2.22) into equation (2.20)

$$i\hbar\left[\dot{\xi}^+\psi_{01}^+ + \xi^+\dot{\psi}_{01}^+ + \left(\frac{H_2\psi_{\mathbf{k}_1} - i\hbar\left[\dot{\xi}^+\psi_{02}^+ + \xi^+\dot{\psi}_{02}^+ + \xi^-\dot{\psi}_{02}^-\right]}{i\hbar\psi_{02}^-}\right)\psi_{01}^- + \xi^-\dot{\psi}_{01}^-\right] = H_1\psi_{\mathbf{k}_2} \tag{2.23}$$

Multiplying both sides by ψ_{02}^- and dividing by $\hbar$:

$$\begin{aligned} i\dot{\xi}^+\psi_{01}^+\psi_{02}^- - i\dot{\xi}^+\psi_{02}^+\psi_{01}^- + i\xi^+\dot{\psi}_{01}^+\psi_{02}^- + \frac{H_2}{\hbar}\psi_{\mathbf{k}_1}\psi_{01}^- \\ - i\xi^+\dot{\psi}_{02}^+\psi_{01}^- - i\xi^-\dot{\psi}_{02}^-\psi_{01}^- + i\xi^-\dot{\psi}_{01}^- = \frac{H_1}{\hbar}\psi_{\mathbf{k}_2} \end{aligned} \tag{2.24}$$

$$\begin{aligned} i\left(\psi_{01}^+\psi_{02}^- - \psi_{02}^+\psi_{01}^-\right)\dot{\xi}^+ = &- i\left(\dot{\psi}_{01}^+\psi_{02}^- - \dot{\psi}_{02}^+\psi_{01}^-\right)\xi^+ \\ &- i\left(\dot{\psi}_{01}^-\psi_{02}^- - \dot{\psi}_{02}^-\psi_{01}^-\right)\xi^- \\ &- \frac{H_2}{\hbar}\psi_{\mathbf{k}_1}\psi_{01}^- \\ &+ \frac{H_1}{\hbar}\psi_{\mathbf{k}_2}\psi_{02}^- \end{aligned} \tag{2.25}$$

To simplify the calculations, we define the following variables

$$\zeta \triangleq \psi_{01}^+\psi_{02}^- - \psi_{02}^+\psi_{01}^- \tag{2.26}$$

$$\delta^+ \triangleq \dot{\psi}_{01}^+\psi_{02}^- - \dot{\psi}_{02}^+\psi_{01}^- \tag{2.27}$$

$$\delta^- \triangleq \dot{\psi}_{01}^-\psi_{02}^- - \dot{\psi}_{02}^-\psi_{01}^- \tag{2.28}$$

Using these definitions in equation (2.25)

$$i\zeta\dot{\xi}^+ = -i\delta^+\xi^+ - i\delta^-\xi^- - \frac{H_2}{\hbar}\left(\xi^+\psi_{01}^+ + \xi^-\psi_{01}^-\right)\psi_{01}^- + \frac{H_1}{\hbar}\left(\xi^+\psi_{02}^+ + \xi^-\psi_{02}^-\right)\psi_{02}^- \tag{2.29}$$

Gathering all terms with ξ^+ and ξ^- together and dividing both sides by ζ:

$$\begin{aligned} i\dot{\xi}^+ = &- \left(i\frac{\delta^+}{\zeta} + \frac{H_2}{\hbar\zeta}\psi_{01}^+\psi_{01}^- - \frac{H_1}{\hbar\zeta}\psi_{02}^+\psi_{02}^-\right)\xi^+ \\ &- \left(i\frac{\delta^-}{\zeta} + \frac{H_2}{\hbar\zeta}\psi_{01}^-\psi_{01}^- - \frac{H_1}{\hbar\zeta}\psi_{02}^-\psi_{02}^-\right)\xi^- \end{aligned} \tag{2.30}$$

Using the following definitions

$$\Delta^+ \triangleq i\frac{\delta^+}{\zeta} + \frac{H_2}{\hbar\zeta}\psi_{01}^+\psi_{01}^- - \frac{H_1}{\hbar\zeta}\psi_{02}^+\psi_{02}^- \tag{2.31}$$

$$\Delta^- \triangleq i\frac{\delta^-}{\zeta} + \frac{H_2}{\hbar\zeta}\psi_{01}^-\psi_{01}^- - \frac{H_1}{\hbar\zeta}\psi_{02}^-\psi_{02}^- \tag{2.32}$$

The equation becomes

$$i\dot{\xi}^+ = -\Delta^+\xi^+ - \Delta^-\xi^- \tag{2.33}$$

Now we need to find Δ^+ and Δ^-. To do this, we first find ζ, δ^+, δ^-, noting that $W_0^2 = \Omega^2 - (\hbar\omega)^2$:

$$\begin{aligned}
\zeta &= \psi_{01}^+\psi_{02}^- - \psi_{02}^+\psi_{01}^- \\
&= -\left(\frac{\Omega+\hbar\omega}{2\Omega}\right) - \left(\frac{\Omega-\hbar\omega}{2\Omega}\right) \\
&= -\left(\frac{\Omega+\hbar\omega}{2\Omega} + \frac{\Omega-\hbar\omega}{2\Omega}\right) \\
\zeta &= -1, \qquad (2.34)\\
\delta^+ &= \dot{\psi}_{01}^+\psi_{02}^- - \dot{\psi}_{02}^+\psi_{01}^- \\
&= -i\left(\frac{\Omega-\hbar\omega}{2\hbar}\right)\left(\frac{\Omega+\hbar\omega}{2\Omega}\right) - i\left(\frac{\Omega+\hbar\omega}{2\hbar}\right)\left(\frac{\Omega-\hbar\omega}{2\Omega}\right) \\
&= -i\frac{1}{4\hbar\Omega}\left[(\Omega-\hbar\omega)(\Omega+\hbar\omega) + (\Omega+\hbar\omega)(\Omega-\hbar\omega)\right] \\
&= -i\frac{(\Omega-\hbar\omega)(\Omega+\hbar\omega)}{2\hbar\Omega} \\
\delta^+ &= -i\frac{W_0^2}{2\hbar\Omega}, \qquad (2.35)\\
\delta^- &= \dot{\psi}_{01}^-\psi_{02}^- - \dot{\psi}_{02}^-\psi_{01}^- \\
&= i\left(\frac{\Omega+\hbar\omega}{4\hbar\Omega}\right)\sqrt{(\Omega-\hbar\omega)(\Omega+\hbar\omega)}e^{-\frac{i\Omega t}{\hbar}} \\
&\quad - i\left(\frac{\Omega-\hbar\omega}{4\hbar\Omega}\right)\sqrt{(\Omega-\hbar\omega)(\Omega+\hbar\omega)}e^{-\frac{i\Omega t}{\hbar}} \\
&= i\frac{\omega}{2\Omega}\sqrt{(\Omega-\hbar\omega)(\Omega+\hbar\omega)}e^{-\frac{i\Omega t}{\hbar}} \\
\delta^- &= i\frac{W_0\omega}{2\Omega}e^{-\frac{i\Omega t}{\hbar}} \qquad (2.36)
\end{aligned}$$

Now we calculate Δ^+:

$$\begin{aligned}\Delta^+ &= i\frac{\delta^+}{\zeta} + \frac{H_2}{\hbar\zeta}\psi_{01}^+\psi_{01}^- - \frac{H_1}{\hbar\zeta}\psi_{02}^+\psi_{02}^- \\ &= b + c - d\end{aligned} \tag{2.37}$$

Calculating b, c and d:

$$\begin{aligned}b &= i\left(-i\frac{W_0^2}{2\hbar\Omega}\right)(-1) \\ b &= -\frac{W_0^2}{2\hbar\Omega}\end{aligned} \tag{2.38}$$

c:

$$\begin{aligned}c &= \frac{H_2}{\hbar\zeta}\psi_{01}^+\psi_{01}^- \\ &= -\frac{1}{\hbar}\left(-\frac{W_0}{2}e^{i\omega t} + \hbar v(k_x + ik_y)\right)\frac{W_0}{2\Omega}e^{-i\omega t} \\ &= -\frac{W_0}{2\Omega}\left(-\frac{W_0}{2\hbar}e^{i\omega t} + v(k_x + ik_y)\right)e^{-i\omega t} \\ &= -\frac{W_0}{2\Omega}\left(-\frac{W_0}{2\hbar} + v(k_x + ik_y)e^{-i\omega t}\right)\end{aligned} \tag{2.39}$$

d:

$$\begin{aligned}d &= \frac{H_1}{\hbar\zeta}\psi_{02}^+\psi_{02}^- \\ &= \frac{1}{\hbar}\left(-\frac{W_0}{2}e^{-i\omega t} + \hbar v(k_x - ik_y)\right)\frac{W_0}{2\Omega}e^{-i\omega t} \\ &= \frac{W_0}{2\Omega}\left(-\frac{W_0}{2\hbar}e^{-i\omega t} + v(k_x - ik_y)\right)e^{i\omega t} \\ &= \frac{W_0}{2\Omega}\left(-\frac{W_0}{2\hbar} + v(k_x - ik_y)e^{i\omega t}\right)\end{aligned} \tag{2.40}$$

$c - d$:

$$\begin{aligned} c - d &= -\frac{W_0}{2\Omega}\left(-\frac{W_0}{2\hbar} + v(k_x + ik_y)e^{-i\omega t} + -\frac{W_0}{2\hbar} + v(k_x - ik_y)e^{i\omega t}\right) \\ &= -\frac{W_0}{2\Omega}\left(-\frac{W_0}{\hbar} + vk_x\left(e^{i\omega t} + e^{-i\omega t}\right) + ivk_y\left(e^{-i\omega t} - e^{i\omega t}\right)\right) \\ &= -\frac{W_0}{2\Omega}\left(-\frac{W_0}{\hbar} + 2v\left(k_x\cos\omega t + k_y\sin\omega t\right)\right) \end{aligned} \tag{2.41}$$

Δ^+:

$$\begin{aligned} \Delta^+ &= b + c - d \\ &= -\frac{W_0^2}{2\hbar\Omega} - \frac{W_0}{2\Omega}\left(-\frac{W_0}{\hbar} + 2v\left(k_x\cos\omega t + k_y\sin\omega t\right)\right) \\ &= -(1-1)\frac{W_0^2}{2\hbar\Omega} - v\frac{W_0}{\Omega}\left(k_x\cos\omega t + k_y\sin\omega t\right) \\ \Delta^+ &= -v\frac{W_0}{\Omega}\left(k_x\cos\omega t + k_y\sin\omega t\right) \end{aligned} \tag{2.42}$$

Now we calculate Δ^-:

$$\begin{aligned} \Delta^- &= i\frac{\delta^-}{\zeta} + \frac{H_2}{\hbar\zeta}\psi_{01}^-\psi_{01}^- - \frac{H_1}{\hbar\zeta}\psi_{02}^-\psi_{02}^- \\ &= f + g - h \end{aligned} \tag{2.43}$$

Calculating f, g and h:

$$\begin{aligned} f &= i\left(i\frac{W_0\omega}{2\Omega}e^{-\frac{i\Omega t}{\hbar}}\right)(-1) \\ &= \frac{W_0\omega}{2\Omega}e^{-\frac{i\Omega t}{\hbar}} \end{aligned} \tag{2.44}$$

g:

$$\begin{aligned} g &= \frac{H_2}{\hbar\zeta}\psi_{01}^-\psi_{01}^- \\ &= -\frac{1}{\hbar}\left(-\frac{W_0}{2}e^{i\omega t} + \hbar v(k_x + ik_y)\right)\left(\frac{\Omega - \hbar\omega}{2\Omega}\right)e^{-\frac{i\Omega t}{\hbar} - i\omega t} \\ &= -\left(-\frac{W_0}{2\hbar}e^{i\omega t} + v(k_x + ik_y)\right)\left(\frac{\Omega - \hbar\omega}{2\Omega}\right)e^{-\frac{i\Omega t}{\hbar} - i\omega t} \\ &= -\left(-\frac{W_0}{2\hbar}e^{-\frac{i\Omega t}{\hbar}} + v(k_x + ik_y)e^{-\frac{i\Omega t}{\hbar} - i\omega t}\right)\left(\frac{\Omega - \hbar\omega}{2\Omega}\right) \end{aligned} \tag{2.45}$$

h:

$$\begin{aligned} h &= \frac{H_1}{\hbar\zeta}\psi_{02}^{-}\psi_{02}^{-} \\ &= -\frac{1}{\hbar}\left(-\frac{W_0}{2}e^{-i\omega t} + \hbar v(k_x - ik_y)\right)\left(\frac{\Omega+\hbar\omega}{2\Omega}\right)e^{-\frac{i\Omega t}{\hbar}+i\omega t} \\ &= -\left(-\frac{W_0}{2\hbar}e^{-i\omega t} + v(k_x - ik_y)\right)\left(\frac{\Omega+\hbar\omega}{2\Omega}\right)e^{-\frac{i\Omega t}{\hbar}+i\omega t} \\ &= -\left(-\frac{W_0}{2\hbar}e^{-\frac{i\Omega t}{\hbar}} + v(k_x - ik_y)e^{-\frac{i\Omega t}{\hbar}+i\omega t}\right)\left(\frac{\Omega+\hbar\omega}{2\Omega}\right) \end{aligned} \tag{2.46}$$

$g - h$:

$$\begin{aligned} g - h = -e^{-\frac{i\Omega t}{\hbar}}&\left[\left(-\frac{W_0}{2\hbar} + v(k_x + ik_y)e^{-i\omega t}\right)\left(\frac{\Omega-\hbar\omega}{2\Omega}\right)\right. \\ &\left.-\left(-\frac{W_0}{2\hbar} + v(k_x - ik_y)e^{i\omega t}\right)\left(\frac{\Omega+\hbar\omega}{2\Omega}\right)\right] \\ = -e^{-\frac{i\Omega t}{\hbar}}&\left[\frac{W_0\omega}{2\Omega} + v(k_x + ik_y)\left(\frac{\Omega-\hbar\omega}{2\Omega}\right)e^{-i\omega t}\right. \\ &\left.- v(k_x - ik_y)\left(\frac{\Omega+\hbar\omega}{2\Omega}\right)e^{i\omega t}\right] \end{aligned} \tag{2.47}$$

Δ^-:

$$\begin{aligned} \Delta^- &= f + g - h \\ &= \frac{W_0\omega}{2\Omega}e^{-\frac{i\Omega t}{\hbar}} - e^{-\frac{i\Omega t}{\hbar}}\left[\frac{W_0\omega}{\Omega} + v(k_x + ik_y)\left(\frac{\Omega-\hbar\omega}{2\Omega}\right)e^{-i\omega t}\right. \\ &\left.- v(k_x - ik_y)\left(\frac{\Omega+\hbar\omega}{2\Omega}\right)e^{i\omega t}\right] \\ &= (1-1)\frac{W_0\omega}{2\Omega}e^{-\frac{i\Omega t}{\hbar}} - v(k_x + ik_y)\left(\frac{\Omega-\hbar\omega}{2\Omega}\right)e^{-i\left(\frac{\Omega}{\hbar}+\omega\right)t} \\ &+ v(k_x - ik_y)\left(\frac{\Omega+\hbar\omega}{2\Omega}\right)e^{-i\left(\frac{\Omega}{\hbar}-\omega\right)t} \\ \Delta^- &= -v(k_x + ik_y)\left(\frac{\Omega-\hbar\omega}{2\Omega}\right)e^{-i\left(\frac{\Omega}{\hbar}+\omega\right)t} + v(k_x - ik_y)\left(\frac{\Omega+\hbar\omega}{2\Omega}\right)e^{-i\left(\frac{\Omega}{\hbar}-\omega\right)t} \end{aligned} \tag{2.48}$$

Finally, subbing equations (2.42) and (2.48) into equation (2.33), we get the following:

$$\begin{aligned} i\dot{\xi}^{+} &= v\left[\frac{W_0}{\Omega}\left(k_x\cos\omega t + k_y\sin\omega t\right)\xi^{+}\right. \\ &\left.-(k_x - ik_y)\left(\frac{\Omega+\hbar\omega}{2\Omega}\right)e^{-i\left(\frac{\Omega}{\hbar}-\omega\right)t}\xi^{-} + (k_x + ik_y)\left(\frac{\Omega-\hbar\omega}{2\Omega}\right)e^{-i\left(\frac{\Omega}{\hbar}+\omega\right)t}\xi^{-}\right] \end{aligned} \tag{2.49}$$

$$\begin{aligned} i\dot{\xi}^{-} &= -v\left[\frac{W_0}{\Omega}\left(k_x\cos\omega t + k_y\sin\omega t\right)\xi^{-}\right. \\ &\left.+(k_x + ik_y)\left(\frac{\Omega+\hbar\omega}{2\Omega}\right)e^{i\left(\frac{\Omega}{\hbar}+\omega\right)t}\xi^{+} - (k_x - ik_y)\left(\frac{\Omega-\hbar\omega}{2\Omega}\right)e^{i\left(\frac{\Omega}{\hbar}-\omega\right)t}\xi^{+}\right] \end{aligned} \tag{2.50}$$

Under high frequency, where the relation $\dfrac{W_0}{\hbar\omega}$ holds, equations (2.49) and (2.50) will simplify with the following:

$$\frac{W_0}{\Omega} \approx \frac{W_0}{\hbar\omega} \approx 0, \frac{\Omega+\hbar\omega}{2\Omega} \approx 1, \frac{\Omega-\hbar\omega}{2\Omega} \approx 0, \tag{2.51}$$

to the following equations [19]:

$$\begin{aligned} i\dot{\xi}^{+}(t) &= -v(k_x - ik_y)e^{-i\left(\frac{\Omega}{\hbar}-\omega\right)t}\xi^{-}(t) \\ i\dot{\xi}^{-}(t) &= -v(k_x + ik_y)e^{i\left(\frac{\Omega}{\hbar}-\omega\right)t}\xi^{+}(t) \end{aligned} \tag{2.52}$$

From here, we take the time derivative of the first equation of these two coupled equations and insert the second equation into the derivative of the first to get a second order equation in terms of ξ^{+}:

$$i\ddot{\xi}^{+} = -v(k_x - ik_y)\left(-i\frac{(\Omega-\hbar\omega)}{\hbar}\right)e^{-i\left(\frac{\Omega}{\hbar}-\omega\right)t}\xi^{-} - v(k_x - ik_y)e^{-i\left(\frac{\Omega}{\hbar}-\omega\right)t}\,\dot{\xi}^{-} \tag{2.53}$$

We have the following:

$$\xi^{-} = -\frac{i\dot{\xi}^{+}}{v(k_x - ik_y)}e^{i\left(\frac{\Omega}{\hbar}-\omega\right)t} \tag{2.54}$$

and

$$\dot{\xi}^{-} = iv(k_x + ik_y)e^{i\left(\frac{\Omega}{\hbar}-\omega\right)t}\xi^{+} \tag{2.55}$$

Inserting the above equations into equation (2.53):

$$\ddot{\xi}^{+}(t) = -i\frac{(\Omega-\hbar\omega)}{\hbar}\dot{\xi}^{+}(t) - (vk)^2\xi^{+}(t) \tag{2.56}$$

We can get both ξ^+ and ξ^- from this equation. First we find ξ^+:

$$\begin{aligned}
\xi^+ &= C^+ e^{-\frac{i}{2}\left(-i\sqrt{-\frac{(\Omega-\hbar\omega)^2}{\hbar^2}-4(vk)^2}+\frac{\Omega-\hbar\omega}{\hbar}\right)t} \\
&= C^+ e^{-\frac{i}{2}\left(-i\sqrt{-(\Omega-\hbar\omega)^2-4(\hbar vk)^2}+\Omega-\hbar\omega\right)\frac{t}{\hbar}} \\
&= C^+ e^{-i\left(-i\sqrt{-\left(\frac{\Omega-\hbar\omega}{2}\right)^2-(\hbar vk)^2}+\frac{\Omega-\hbar\omega}{2}\right)\frac{t}{\hbar}} \\
&= C^+ e^{-i\left(\sqrt{\left(\frac{\Omega-\hbar\omega}{2}\right)^2+(\hbar vk)^2}+\frac{\Omega}{2}-\frac{\hbar\omega}{2}\right)\frac{t}{\hbar}}
\end{aligned} \tag{2.57}$$

Similarly for ξ^-:

$$\begin{aligned}
\xi^- &= C^- e^{\frac{i}{2}\left(-i\sqrt{-\frac{(\Omega-\hbar\omega)^2}{\hbar^2}-4(vk)^2}-\frac{\Omega-\hbar\omega}{\hbar}\right)t} \\
&= C^- e^{-\frac{i}{2}\left(i\sqrt{-(\Omega-\hbar\omega)^2-4(\hbar vk)^2}-\Omega-\hbar\omega\right)\frac{t}{\hbar}} \\
&= C^- e^{-i\left(i\sqrt{-\left(\frac{\Omega-\hbar\omega}{2}\right)^2-(\hbar vk)^2}-\frac{\Omega-\hbar\omega}{2}\right)\frac{t}{\hbar}} \\
&= C^- e^{-i\left(-\sqrt{\left(\frac{\Omega-\hbar\omega}{2}\right)^2+(\hbar vk)^2}-\frac{\Omega}{2}+\frac{\hbar\omega}{2}\right)\frac{t}{\hbar}}
\end{aligned} \tag{2.58}$$

We make the following definition:

$$\varepsilon_{\mathbf{k}} = \sqrt{\left(\frac{\Omega-\hbar\omega}{2}\right)^2+(\hbar vk)^2} \tag{2.59}$$

or written a different way:

$$\varepsilon_{\mathbf{k}} = \sqrt{\left(\frac{\varepsilon_g}{2}\right)^2+(\hbar vk)^2} \tag{2.60}$$

where:

$$\begin{aligned}
\varepsilon_g &= \sqrt{(\hbar\omega)^2+\left(\frac{2veE_0}{\omega}\right)^2}-\hbar\omega \\
&= \hbar\omega_{\text{dressed}}-\hbar\omega \\
&= \hbar(\omega_{\text{dressed}}-\omega)
\end{aligned} \tag{2.61}$$

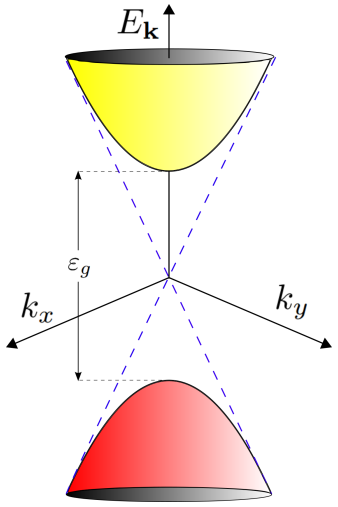

Figure 2.4: Gap created at the location of the Dirac cones, with a magnitude of ε_g.

The immediate result of this energy dispersion is the opening of a gap at the Dirac points as shown in Figure 2.4. (compare with Figure 1.2.) The energy gap can be expressed in terms of the difference between the dressed and the original frequency multiplied by $\hbar$. It is similar to the detuning for the generalized Rabi frequency of a two-level system.

Now we can write ξ^+ and ξ^- in the following form:

$$\xi^{\pm}(t) = C^{\pm} e^{-i\left(\pm\frac{\Omega}{2}\mp\frac{\hbar\omega}{2}+\varepsilon_{\mathbf{k}}\right)\frac{t}{\hbar}} \tag{2.62}$$

To find C^+ and C^-, we must make use of the normalization condition for the wavefunction $\psi_{\mathbf{k}}$:

$$\begin{aligned} 1 &= \langle\psi_{\mathbf{k}}|\psi_{\mathbf{k}}\rangle \\ &= |\xi^+|^2 \langle\psi_0^+|\psi_0^+\rangle + |\xi^-|^2 \langle\psi_0^-|\psi_0^-\rangle \\ &= |\xi^+|^2 + |\xi^-|^2 \\ &= \left|C^+ e^{-i\left(\frac{\Omega}{2}-\frac{\hbar\omega}{2}+\varepsilon_{\mathbf{k}}\right)\frac{t}{\hbar}}\right|^2 + \left|C^- e^{-i\left(-\frac{\Omega}{2}+\frac{\hbar\omega}{2}-\varepsilon_{\mathbf{k}}\right)\frac{t}{\hbar}}\right|^2 \\ 1 &= |C^+|^2 + |C^-|^2 \end{aligned} \tag{2.63}$$

Now using this result alongside the first equation in (2.52), the left hand side will be:

$$\begin{aligned} i\dot{\xi}^+ &= i\left(C^+\left(-\frac{i}{\hbar}\left(\frac{\Omega}{2}-\frac{\hbar\omega}{2}+\varepsilon_{\mathbf{k}}\right)\right)e^{-i\left(\frac{\Omega}{2}-\frac{\hbar\omega}{2}+\varepsilon_{\mathbf{k}}\right)\frac{t}{\hbar}}\right) \\ &= C^+\frac{1}{\hbar}\left(\frac{\Omega}{2}-\frac{\hbar\omega}{2}+\varepsilon_{\mathbf{k}}\right)e^{-i\left(\frac{\Omega}{2}-\frac{\hbar\omega}{2}+\varepsilon_{\mathbf{k}}\right)\frac{t}{\hbar}} \end{aligned} \tag{2.64}$$

The right hand side will be:

$$= -v(k_x - ik_y)e^{-i\frac{(\Omega-\hbar\omega)}{\hbar}t}C^- e^{-i\left(-\frac{\Omega}{2}+\frac{\hbar\omega}{2}-\varepsilon_{\mathbf{k}}\right)\frac{t}{\hbar}} \tag{2.65}$$

At $t = 0$, we will have the following equation:

$$C^+\frac{1}{\hbar}\left(\frac{\Omega}{2} - \frac{\hbar\omega}{2} + \varepsilon_{\mathbf{k}}\right) = -v(k_x - ik_y)C^- \tag{2.66}$$

Taking the magnitude squared of both sides:

$$\begin{aligned}
\left|C^+\frac{1}{\hbar}\left(\frac{\Omega}{2} - \frac{\hbar\omega}{2} + \varepsilon_{\mathbf{k}}\right)\right|^2 &= \left|-v(k_x - ik_y)C^-\right|^2 \\
\left|C^+\right|^2\frac{1}{\hbar^2}\left(\frac{\Omega}{2} - \frac{\hbar\omega}{2} + \varepsilon_{\mathbf{k}}\right)^2 &= (vk)^2\left|C^-\right|^2 \\
\left|C^+\right|^2\frac{1}{\hbar^2}\left(\frac{\varepsilon_g}{2} + \varepsilon_{\mathbf{k}}\right)^2 &= (vk)^2\left|C^-\right|^2
\end{aligned} \tag{2.67}$$

Now we use the normalization condition obtained previously ($|C^-|^2 = 1 - |C^+|^2$):

$$\begin{aligned}
\left|C^+\right|^2\frac{1}{\hbar^2}\left(\frac{\varepsilon_g}{2} + \varepsilon_{\mathbf{k}}\right)^2 &= (vk)^2\left(1 - \left|C^+\right|^2\right) \\
\left|C^+\right|^2\frac{1}{\hbar^2}\left(\frac{\varepsilon_g}{2} + \varepsilon_{\mathbf{k}}\right)^2 &= (vk)^2 - (vk)^2\left|C^+\right|^2 \\
\left|C^+\right|^2\frac{1}{\hbar^2}\left(\frac{\varepsilon_g}{2} + \varepsilon_{\mathbf{k}}\right)^2 + (vk)^2\left|C^+\right|^2 &= (vk)^2 \\
\left|C^+\right|^2\left(\frac{\varepsilon_g}{2} + \varepsilon_{\mathbf{k}}\right)^2 + (\hbar vk)^2\left|C^+\right|^2 &= (\hbar vk)^2 \\
\left|C^+\right|^2 &= \frac{(\hbar vk)^2}{\left(\frac{\varepsilon_g}{2} + \varepsilon_{\mathbf{k}}\right)^2 + (\hbar vk)^2} \\
\left|C^+\right|^2 &= \frac{\varepsilon_{\mathbf{k}}^2 - \left(\frac{\varepsilon_g}{2}\right)^2}{\left(\frac{\varepsilon_g}{2}\right)^2 + \varepsilon_{\mathbf{k}}^2 + \varepsilon_g\varepsilon_{\mathbf{k}} + (\hbar vk)^2} \\
\left|C^+\right|^2 &= \frac{\left(\varepsilon_{\mathbf{k}} - \frac{\varepsilon_g}{2}\right)\left(\varepsilon_{\mathbf{k}} + \frac{\varepsilon_g}{2}\right)}{2\varepsilon_{\mathbf{k}}\left(\varepsilon_{\mathbf{k}} + \frac{\varepsilon_g}{2}\right)} \\
\left|C^+\right|^2 &= \frac{\varepsilon_{\mathbf{k}} - \frac{\varepsilon_g}{2}}{2\varepsilon_{\mathbf{k}}} \\
C^+ &= \pm\sqrt{\frac{\varepsilon_{\mathbf{k}} - \frac{\varepsilon_g}{2}}{2\varepsilon_{\mathbf{k}}}}
\end{aligned} \tag{2.68}$$

From this result, we can simply find C^- using the normalization condition:

$$C^- = \mp\sqrt{\frac{\varepsilon_{\mathbf{k}} + \frac{\varepsilon_g}{2}}{2\varepsilon_{\mathbf{k}}}} \tag{2.69}$$

Solving for C^+ and C^- using the second equation in (2.52) will result in the following:

$$C^+ = \pm\sqrt{\frac{\varepsilon_{\mathbf{k}} + \frac{\varepsilon_g}{2}}{2\varepsilon_{\mathbf{k}}}} \tag{2.70}$$

$$C^- = \mp\sqrt{\frac{\varepsilon_{\mathbf{k}} - \frac{\varepsilon_g}{2}}{2\varepsilon_{\mathbf{k}}}} \tag{2.71}$$

So we have four solutions for these constants which come in pairs. We can express the final result as such:

$$C^+ = \pm\sqrt{\frac{\varepsilon_{\mathbf{k}} \mp \frac{\varepsilon_g}{2}}{2\varepsilon_{\mathbf{k}}}} \tag{2.72}$$

$$C^- = \mp\sqrt{\frac{\varepsilon_{\mathbf{k}} \pm \frac{\varepsilon_g}{2}}{2\varepsilon_{\mathbf{k}}}} \tag{2.73}$$

We must note that since we have used the normalization condition, and since C^+ and C^- are complex numbers, we have lost the information of their complex phase. To account for it, we must add this phase in the expression and find it using equation (2.52):

$$C^+ = \pm\sqrt{\frac{\varepsilon_{\mathbf{k}} \mp \frac{\varepsilon_g}{2}}{2\varepsilon_{\mathbf{k}}}} e^{i\theta_1} \tag{2.74}$$

$$C^- = \mp\sqrt{\frac{\varepsilon_{\mathbf{k}} \pm \frac{\varepsilon_g}{2}}{2\varepsilon_{\mathbf{k}}}} e^{i\theta_2} \tag{2.75}$$

Subbing these expressions into equation (2.52):

$$C^+ \frac{1}{\hbar}\left(\frac{\Omega}{2} - \frac{\hbar\omega}{2} + \varepsilon_{\mathbf{k}}\right) e^{-i\frac{\varepsilon_{\mathbf{k}}}{\hbar}t} = -v(k_x - ik_y) e^{-i\frac{(\Omega-\hbar\omega)}{\hbar}t} e^{-i\left(\frac{-\Omega}{2} + \frac{\hbar\omega}{2} - \varepsilon_{\mathbf{k}}\right)\frac{t}{\hbar}} C^- \tag{2.76}$$

Setting t = 0 and substituting the expressions for C^+ and C^-:

$$\sqrt{\frac{\varepsilon_{\mathbf{k}} - \frac{\varepsilon_g}{2}}{2\varepsilon_{\mathbf{k}}}} e^{i\theta_1} \frac{1}{\hbar}\left(\frac{\Omega}{2} - \frac{\hbar\omega}{2} + \varepsilon_{\mathbf{k}}\right) = -v(k_x - ik_y)\left(-\sqrt{\frac{\varepsilon_{\mathbf{k}} + \frac{\varepsilon_g}{2}}{2\varepsilon_{\mathbf{k}}}} e^{i\theta_2}\right) \tag{2.77}$$

Multiplying both sides by $\sqrt{\frac{\varepsilon_{\mathbf{k}}+\frac{\varepsilon_g}{2}}{2\varepsilon_{\mathbf{k}}}}$:

$$\begin{aligned}
\sqrt{\varepsilon_{\mathbf{k}}^2-\left(\frac{\varepsilon_g}{2}\right)^2}e^{i\theta_1}\left(\frac{\Omega}{2}-\frac{\hbar\omega}{2}+\varepsilon_{\mathbf{k}}\right) &= \hbar v(k_x-ik_y)\left(\varepsilon_{\mathbf{k}}+\frac{\varepsilon_g}{2}\right)e^{i\theta_2} \\
(\hbar vk)e^{i\theta_1}\left(\frac{\varepsilon_g}{2}+\varepsilon_{\mathbf{k}}\right) &= (\hbar vk)e^{-i\varphi}\left(\varepsilon_{\mathbf{k}}+\frac{\varepsilon_g}{2}\right)e^{i\theta_2} \\
e^{i\theta_1} &= e^{-i\varphi}e^{i\theta_2} \\
e^{i(\theta_2-\theta_1)} &= e^{i\varphi} \\
\theta_2-\theta_1 &= \varphi
\end{aligned} \tag{2.78}$$

We have found the relation between the phases of C^+ and C^-. We set $\theta_1=-\frac{\varphi}{2}$ and $\theta_2=\frac{\varphi}{2}$. Now we can express the full form of the wavefunction $\psi_{\mathbf{k}}$ using our results:

$$\begin{aligned}
\psi_{\mathbf{k}} = e^{-i\frac{\varepsilon_{\mathbf{k}}}{\hbar}t}\Bigg[&\pm\sqrt{\frac{|\varepsilon_{\mathbf{k}}|\mp\frac{\varepsilon_g}{2}}{2|\varepsilon_{\mathbf{k}}|}}e^{-i\frac{\varphi}{2}}\left(\sqrt{\frac{\Omega+\hbar\omega}{2\Omega}}\Phi_1'(\mathbf{r})+\sqrt{\frac{\Omega-\hbar\omega}{2\Omega}}\Phi_2'(\mathbf{r})e^{i\omega t}\right) \\
&\mp\sqrt{\frac{|\varepsilon_{\mathbf{k}}|\pm\frac{\varepsilon_g}{2}}{2|\varepsilon_{\mathbf{k}}|}}e^{i\frac{\varphi}{2}}\left(\sqrt{\frac{\Omega-\hbar\omega}{2\Omega}}\Phi_1'(\mathbf{r})e^{-i\omega t}-\sqrt{\frac{\Omega+\hbar\omega}{2\Omega}}\Phi_2'(\mathbf{r})\right)\Bigg]
\end{aligned} \tag{2.79}$$

The $+$ and $-$ correspond to the wavefunction for the conduction band and the valence band respectively. This also holds for the sign of $\varepsilon_{\mathbf{k}}$ (this detail is important for when we calculate expectation values using this total wavefunction.)

Setting $\Phi_{1,2}'(\mathbf{r})=\Phi_{1,2}(\mathbf{r})\varphi_{\mathbf{k}}(\mathbf{r})$ and applying the previous approximation in (2.51):

$$\psi_{\mathbf{k}}=\varphi_{\mathbf{k}}(\mathbf{r})e^{-i\frac{\varepsilon_{\mathbf{k}}}{\hbar}t}\left[\pm\sqrt{\frac{|\varepsilon_{\mathbf{k}}|\mp\frac{\varepsilon_g}{2}}{2|\varepsilon_{\mathbf{k}}|}}e^{-i\frac{\varphi}{2}}\Phi_1(\mathbf{r})\pm\sqrt{\frac{|\varepsilon_{\mathbf{k}}|\pm\frac{\varepsilon_g}{2}}{2|\varepsilon_{\mathbf{k}}|}}e^{i\frac{\varphi}{2}}\Phi_2(\mathbf{r})\right] \tag{2.80}$$

This equation is physically equivalent to Eq (2.79), only simplified with the aforementioned approximations which removes all $\sqrt{\frac{\Omega+\hbar\omega}{2\Omega}}$, $\sqrt{\frac{\Omega-\hbar\omega}{2\Omega}}$, $e^{i\omega t}$ and $e^{-i\omega t}$ terms. Both equations refer to the total wavefunction for electrons in the graphene sheet around the K point for the conduction and valence bands.

2.2 Magnetization Formula Applied to Wavefunction

Following the definition of magnetization developed in the paper by Majedi, A. Hamed and Lounis, Brahim [23], we define the formula (ignoring the spin term) for the expectation

value of the magnetization as

$$\langle \hat{\mathbf{M}} \rangle = \frac{Ne}{2m} \langle \hat{\mathbf{L}} \rangle \tag{2.81}$$

where N is the atomic number density of the material ($3.82 \times 10^{19}\,\mathrm{m}^{-2}$ for graphene). Note that the angular momentum operator $\hat{\mathbf{L}}$ is the total angular momentum operator which includes the angular momentum induced from the vector potential of the light. First we write our wavefunction from the previous section (from Eq (2.80)):

$$\psi_{\mathbf{k}} = \varphi_{\mathbf{k}}(\mathbf{r}) e^{-i\frac{\varepsilon_{\mathbf{k}}}{\hbar}t} \left[\sqrt{\frac{|\varepsilon_{\mathbf{k}}| - \frac{\varepsilon_g}{2}}{2|\varepsilon_{\mathbf{k}}|}} e^{-i\frac{\varphi}{2}} \Phi_1(\mathbf{r}) + \sqrt{\frac{|\varepsilon_{\mathbf{k}}| + \frac{\varepsilon_g}{2}}{2|\varepsilon_{\mathbf{k}}|}} e^{i\frac{\varphi}{2}} \Phi_2(\mathbf{r}) \right] \tag{2.82}$$

$$\psi^*_{\mathbf{k}} = \varphi^*_{\mathbf{k}}(\mathbf{r}) e^{i\frac{\varepsilon_{\mathbf{k}}}{\hbar}t} \left[\sqrt{\frac{|\varepsilon_{\mathbf{k}}| - \frac{\varepsilon_g}{2}}{2|\varepsilon_{\mathbf{k}}|}} e^{i\frac{\varphi}{2}} \Phi^*_1(\mathbf{r}) + \sqrt{\frac{|\varepsilon_{\mathbf{k}}| + \frac{\varepsilon_g}{2}}{2|\varepsilon_{\mathbf{k}}|}} e^{-i\frac{\varphi}{2}} \Phi^*_2(\mathbf{r}) \right] \tag{2.83}$$

Using the formula for magnetization as follows [23]:

$$\begin{aligned} \langle \hat{\mathbf{M}} \rangle &= \frac{Ne}{2m} \int \psi^*_{\mathbf{k}} \hat{\mathbf{L}} \psi_{\mathbf{k}} \, d^3\mathbf{r} \\ &= \frac{Ne}{2m} \Big[M_1 I_{11} + M_2 I_{12} + M_3 I_{21} + M_4 I_{22} \Big] \end{aligned} \tag{2.84}$$

where we have the following terms which come from the multiplication of the constant terms attached to the basis functions

$$M_1 = \frac{|\varepsilon_{\mathbf{k}}| - \frac{\varepsilon_g}{2}}{2|\varepsilon_{\mathbf{k}}|} \tag{2.85}$$

$$M_2 = \frac{\hbar v k}{2|\varepsilon_{\mathbf{k}}|} e^{i\varphi} \tag{2.86}$$

$$M_3 = \frac{\hbar v k}{2|\varepsilon_{\mathbf{k}}|} e^{-i\varphi} \tag{2.87}$$

$$M_4 = \frac{|\varepsilon_{\mathbf{k}}| + \frac{\varepsilon_g}{2}}{2|\varepsilon_{\mathbf{k}}|} \tag{2.88}$$

and I_{11}, I_{12}, I_{21} and I_{22} are the integral terms arising from the expectation value of the angular momentum operator with basis functions as the wavefunctions. Although the calculation for all of the M_i terms are not given for the unsimplified wavefunction from Eq (2.79), the final results of the calculation are given and used in the last section of the theoretical analysis.

2.3 Calculation of Expectation Value of Angular Momentum Operator

We note that in this case, the angular momentum operator is:

$$\hat{\mathbf{L}} = \mathbf{r} \times (\mathbf{p} - e\mathbf{A}) \tag{2.89}$$

which can be written as

$$\hat{\mathbf{L}} = \hat{\mathbf{L}}_p + \hat{\mathbf{L}}_A \tag{2.90}$$

where we have

$$\begin{aligned} \hat{\mathbf{L}}_p &= \mathbf{r} \times \mathbf{p} \\ &= \left(\hat{L}_{p_x}, \hat{L}_{p_y}, \hat{L}_{p_z}\right) \end{aligned} \tag{2.91}$$

$$\hat{L}_{p_x} = -i\hbar \left(y\frac{\partial}{\partial z} - z\frac{\partial}{\partial y} \right) \tag{2.92}$$

$$\hat{L}_{p_y} = -i\hbar \left(z\frac{\partial}{\partial x} - x\frac{\partial}{\partial z} \right) \tag{2.93}$$

$$\hat{L}_{p_z} = -i\hbar \left(x\frac{\partial}{\partial y} - y\frac{\partial}{\partial x} \right) \tag{2.94}$$

and

$$\begin{aligned} \hat{\mathbf{L}}_A &= -e\mathbf{r} \times \mathbf{A} \\ &= \left(\hat{L}_{A_x}, \hat{L}_{A_y}, \hat{L}_{A_z}\right) \end{aligned} \tag{2.95}$$

$$\hat{L}_{A_x} = eA_0 z \sin\omega t \tag{2.96}$$

$$\hat{L}_{A_y} = -eA_0 z \cos\omega t \tag{2.97}$$

$$\hat{L}_{A_z} = -eA_0(x \sin\omega t - y \cos\omega t) \tag{2.98}$$

We take the position vector and the wavevector to be:

$$\mathbf{r} = \hat{x}x + \hat{y}y + \hat{z}z \tag{2.99}$$

$$\mathbf{k} = \hat{x}k\cos\varphi + \hat{y}k\sin\varphi \tag{2.100}$$

We also know the formula for the p_z orbital for the carbon atom from the hydrogen atom model:

$$\begin{aligned}\Psi_{210}(\mathbf{r}) &= \frac{1}{\sqrt{32\pi}}\left(\frac{6}{a_0}\right)^{5/2} re^{-\frac{3r}{a_0}}\cos\theta \\ &= \frac{1}{\sqrt{32\pi}}\left(\frac{6}{a_0}\right)^{5/2} ze^{-\frac{3}{a_0}\sqrt{x^2+y^2+z^2}}\end{aligned} \tag{2.101}$$

where a_0 is the Bohr radius. Now we find the expanded form of $\varphi_{\mathbf{k}}(\mathbf{r})$ which is simply the form of the Bloch wavefunction with a normalization factor of S. Usually, this factor is V, but since we are dealing with a 2D material, this factor is a surface area instead:

$$\begin{aligned}\varphi_{\mathbf{k}}(\mathbf{r}) &= \frac{1}{\sqrt{S}}e^{i\mathbf{k}\cdot\mathbf{r}} \\ &= \frac{1}{\sqrt{S}}e^{ik(x\cos\varphi + y\sin\varphi)} \\ &= \frac{1}{\sqrt{S}}e^{ik\sqrt{x^2+y^2}}\end{aligned} \tag{2.102}$$

However, since we are dealing with only one unit cell in our calculations, we normalize S and remove it from calculations. Relating the orbital function to our basic functions, we have (the positions of the atoms are shown with respect to our chosen coordinates in Figure 2.5) [29]:

$$\begin{aligned}\Phi_1(\mathbf{r}) &= e^{i\mathbf{k}\cdot\mathbf{R}_A}\Psi_{210}(\mathbf{r}-\mathbf{R}_A) \\ \Phi_2(\mathbf{r}) &= e^{i\mathbf{k}\cdot\mathbf{R}_B}\Psi_{210}(\mathbf{r}-\mathbf{R}_B)\end{aligned} \tag{2.103}$$

where we have

$$\mathbf{R}_A = -\frac{a_l}{2\sqrt{3}}\hat{x} \tag{2.104}$$

$$\mathbf{R}_B = \frac{a_l}{2\sqrt{3}}\hat{x} \tag{2.105}$$

where $a_l = 2.46$Å is the lattice constant of the graphene honeycomb lattice. Note that $|\mathbf{R}_A| = |\mathbf{R}_B|$ is half of the distance between two adjacent A and B sublattice carbon atoms. From section 1, we can write $|\mathbf{R}_A| = |\mathbf{R}_B| = a/2$. Figures 2.6a and 2.6b show the probability density of the orbitals with their respective shifts.

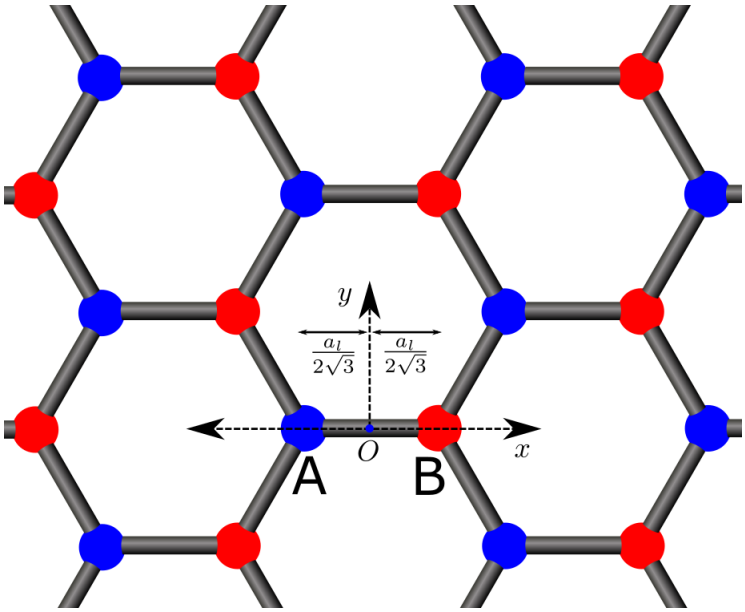

Figure 2.5: Coordinate reference frame for the shifts in the orbital functions.

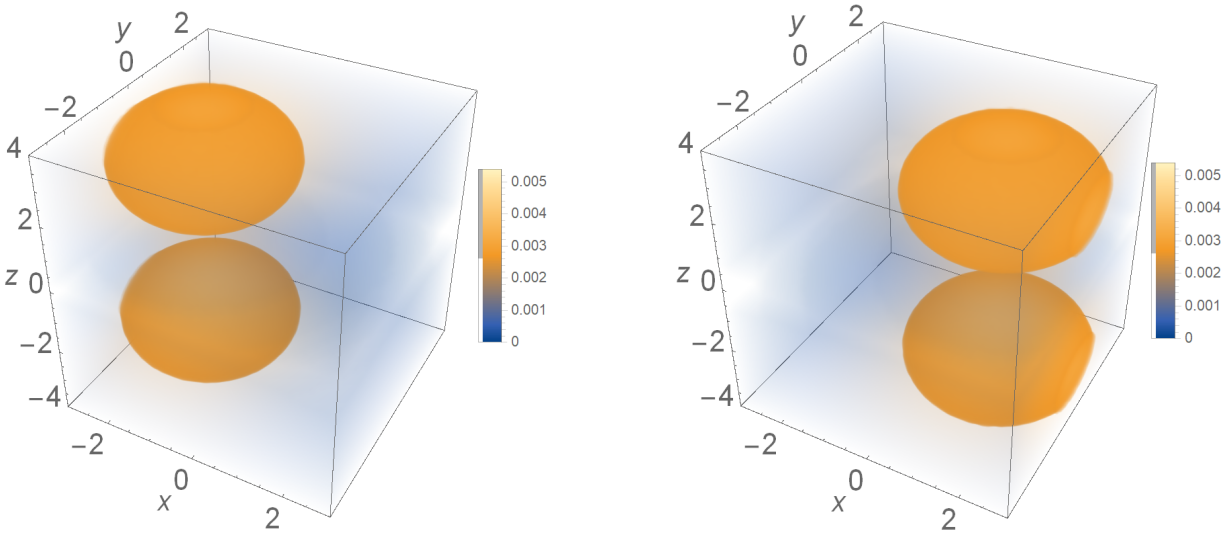

(a) (b)

Figure 2.6: Orbital probability density for a shift in the direction of (a) $\mathbf{R}_A$, (b) $\mathbf{R}_B$.

It is important to note that since these exponential functions are only there to satisfy the Bloch form for the wavefunction in the crystal, they will not be included in the integration process for the inner product of states. Combining these results we will have:

$$\begin{aligned}
\Phi_1(\mathbf{r})\varphi_{\mathbf{k}}(\mathbf{r}) &= \frac{1}{\sqrt{32\pi}}\left(\frac{6}{a_0}\right)^{5/2} z e^{-\frac{3}{a_0}\sqrt{\left(x+\frac{a}{2\sqrt{3}}\right)^2+y^2+z^2}} e^{i\mathbf{k}\cdot\mathbf{R}_A} e^{ik\sqrt{x^2+y^2}} \\
\Phi_1^*(\mathbf{r})\varphi_{\mathbf{k}}^*(\mathbf{r}) &= \frac{1}{\sqrt{32\pi}}\left(\frac{6}{a_0}\right)^{5/2} z e^{-\frac{3}{a_0}\sqrt{\left(x+\frac{a}{2\sqrt{3}}\right)^2+y^2+z^2}} e^{-i\mathbf{k}\cdot\mathbf{R}_A} e^{-ik\sqrt{x^2+y^2}}
\end{aligned} \tag{2.106}$$

$$\begin{aligned}
\Phi_2(\mathbf{r})\varphi_{\mathbf{k}}(\mathbf{r}) &= \frac{1}{\sqrt{32\pi}}\left(\frac{6}{a_0}\right)^{5/2} z e^{-\frac{3}{a_0}\sqrt{\left(x-\frac{a}{2\sqrt{3}}\right)^2+y^2+z^2}} e^{i\mathbf{k}\cdot\mathbf{R}_B} e^{ik\sqrt{x^2+y^2}} \\
\Phi_2^*(\mathbf{r})\varphi_{\mathbf{k}}^*(\mathbf{r}) &= \frac{1}{\sqrt{32\pi}}\left(\frac{6}{a_0}\right)^{5/2} z e^{-\frac{3}{a_0}\sqrt{\left(x-\frac{a}{2\sqrt{3}}\right)^2+y^2+z^2}} e^{-i\mathbf{k}\cdot\mathbf{R}_B} e^{-ik\sqrt{x^2+y^2}}
\end{aligned} \tag{2.107}$$

The integrals from the angular momentum operator $\hat{\mathbf{L}}_p$ are very straightforward. Since we know that

$$\hat{L}_z|\psi_{nlm}\rangle = m\hbar|\psi_{nlm}\rangle \tag{2.108}$$

Since $m = 0$ for the $2p_z$ orbital, the resulting expectation value will also be zero. This is a very predictable result since it states that expectation value of the angular momentum for the $2p_z$ orbitals are zero. We have also carried out the integral calculations for the $\hat{\mathbf{L}}_p$ expectation values as an extra check and confirmed that they are all zero (we do not include these calculations here.) Essentially, it means that any nonzero expectation for the angular momentum operator with the $2p_z$ orbitals has to come from the angular momentum imparted by light, or in other words, the canonical momentum.

We will have the following integrals (note that $I_{12} = I_{21}$):

$$I_{11} = \int \Phi_1^*(\mathbf{r})\varphi_{\mathbf{k}}^*(\mathbf{r})\hat{L}_A\Big[\Phi_1(\mathbf{r})\varphi_{\mathbf{k}}(\mathbf{r})\Big]\, d^3\mathbf{r} \tag{2.109}$$

$$I_{12} = \int \Phi_1^*(\mathbf{r})\varphi_{\mathbf{k}}^*(\mathbf{r})\hat{L}_A\Big[\Phi_2(\mathbf{r})\varphi_{\mathbf{k}}(\mathbf{r})\Big]\, d^3\mathbf{r} \tag{2.110}$$

$$I_{22} = \int \Phi_2^*(\mathbf{r})\varphi_{\mathbf{k}}^*(\mathbf{r})\hat{L}_A\Big[\Phi_2(\mathbf{r})\varphi_{\mathbf{k}}(\mathbf{r})\Big]\, d^3\mathbf{r} \tag{2.111}$$

We will need to solve these integrals numerically with Matlab (refer to Appendix B).

$$\begin{aligned} I_{11_x} &= \int \Phi_1^*(\mathbf{r})\varphi_{\mathbf{k}}^*(\mathbf{r})(-eA_0 z\sin\omega t)\Big[\Phi_1(\mathbf{r})\varphi_{\mathbf{k}}(\mathbf{r})\Big]\,d^3\mathbf{r} \\ &= (-eA_0\sin\omega t)\frac{1}{32\pi}\left(\frac{6}{a_0}\right)^5\int_{-\infty}^{\infty}\int_{-\infty}^{\infty}\int_{-\infty}^{\infty} z^3 e^{-\frac{6}{a_0}\sqrt{(x-\mathbf{R}_A)^2+y^2+z^2}}\,dx\,dy\,dz \end{aligned} \tag{2.112}$$

$$\begin{aligned} I_{11_y} &= \int \Phi_1^*(\mathbf{r})\varphi_{\mathbf{k}}^*(\mathbf{r})(-eA_0 z\cos\omega t)\Big[\Phi_1(\mathbf{r})\varphi_{\mathbf{k}}(\mathbf{r})\Big]\,d^3\mathbf{r} \\ &= (-eA_0\cos\omega t)\frac{1}{32\pi}\left(\frac{6}{a_0}\right)^5\int_{-\infty}^{\infty}\int_{-\infty}^{\infty}\int_{-\infty}^{\infty} z^3 e^{-\frac{6}{a_0}\sqrt{(x-\mathbf{R}_A)^2+y^2+z^2}}\,dx\,dy\,dz \end{aligned} \tag{2.113}$$

$$\begin{aligned} I_{11_z} &= \int \Phi_1^*(\mathbf{r})\varphi_{\mathbf{k}}^*(\mathbf{r})(-eA_0 x\sin\omega t + eA_0 y\cos\omega t)\Big[\Phi_1(\mathbf{r})\varphi_{\mathbf{k}}(\mathbf{r})\Big]\,d^3\mathbf{r} \\ &= (-eA_0\sin\omega t)\frac{1}{32\pi}\left(\frac{6}{a_0}\right)^5\int_{-\infty}^{\infty}\int_{-\infty}^{\infty}\int_{-\infty}^{\infty} xz^2 e^{-\frac{6}{a_0}\sqrt{(x-\mathbf{R}_A)^2+y^2+z^2}}\,dx\,dy\,dz \\ &+ (eA_0\cos\omega t)\frac{1}{32\pi}\left(\frac{6}{a_0}\right)^5\int_{-\infty}^{\infty}\int_{-\infty}^{\infty}\int_{-\infty}^{\infty} yz^2 e^{-\frac{6}{a_0}\sqrt{(x-\mathbf{R}_A)^2+y^2+z^2}}\,dx\,dy\,dz \end{aligned} \tag{2.114}$$

With the exception of I_{11_z} and I_{22_z}, all of the integrals are zero:

$$I_{11_z} = -\frac{a}{2}eA_0\sin\omega t \tag{2.115}$$

$$I_{22_z} = \frac{a}{2}eA_0\sin\omega t \tag{2.116}$$

If we use equations (2.84) and (2.85)–(2.88), we will have the following:

$$\begin{aligned} \langle\hat{\mathbf{M}}\rangle_z &= \frac{Ne}{2m}\left[\left(\frac{|\varepsilon_{\mathbf{k}}|-\frac{\varepsilon_g}{2}}{2|\varepsilon_{\mathbf{k}}|}\right)\left(-\frac{a}{2}eA_0\sin\omega t\right)+\left(\frac{|\varepsilon_{\mathbf{k}}|+\frac{\varepsilon_g}{2}}{2|\varepsilon_{\mathbf{k}}|}\right)\left(\frac{a}{2}eA_0\sin\omega t\right)\right] \\ &= \frac{Na\,e}{4m}eA_0\sin\omega t\left[\left(-\frac{|\varepsilon_{\mathbf{k}}|-\frac{\varepsilon_g}{2}}{2|\varepsilon_{\mathbf{k}}|}\right)+\left(\frac{|\varepsilon_{\mathbf{k}}|+\frac{\varepsilon_g}{2}}{2|\varepsilon_{\mathbf{k}}|}\right)\right] \\ &= \frac{Na\,e}{4m}eA_0\sin\omega t\frac{\varepsilon_g}{2|\varepsilon_{\mathbf{k}}|} \\ \langle\hat{\mathbf{M}}\rangle_z &= \frac{Ne^2aE_0}{8m\omega}\frac{\varepsilon_g}{|\varepsilon_{\mathbf{k}}|}\sin\omega t \end{aligned} \tag{2.117}$$

This result clearly has no DC components. In order to get the magnetization with non-zero DC component, we will have to use the unsimplified wavefunction from Eq (2.79) where

the approximations in Eq (2.51) are not applied to the wavefunction itself. This will yield the following:

$$\begin{aligned}\langle\hat{\mathbf{M}}\rangle_z &= \frac{Ne}{2m}\left[\frac{\hbar\omega}{\Omega}\frac{\varepsilon_g}{2|\varepsilon_{\mathbf{k}}|} - \frac{\hbar vk}{|\varepsilon_{\mathbf{k}}|}\frac{W_0}{\Omega}\cos\left(-\omega t+\varphi\right)\right] I_{11_z} \\ &= -\frac{Ne^2a\hbar E_0}{4m\omega|\varepsilon_{\mathbf{k}}|\Omega}\left[\frac{\omega\varepsilon_g}{2} - \frac{2ev^2kE_0}{\omega}\cos\left(-\omega t+\varphi\right)\right]\sin\omega t \end{aligned} \tag{2.118}$$

Therefore, the total magnetization will be:

$$\boxed{\langle\hat{\mathbf{M}}\rangle_z = -\frac{Ne^2a\hbar\,\varepsilon_g E_0}{8m|\varepsilon_{\mathbf{k}}|\Omega}\sin\omega t + \frac{Ne^3a\hbar v^2kE_0^2}{4m\omega^2|\varepsilon_{\mathbf{k}}|\Omega}\Big[\sin\varphi + \sin\left(2\omega t-\varphi\right)\Big]} \tag{2.119}$$

The DC components of the magnetization in the z-direction will then be (the $+z$-direction is in the direction of the propagation of the polarized light):

$$\boxed{\langle\hat{\mathbf{M}}\rangle_{\mathrm{DC}} = \frac{Ne^3a\hbar v^2k\sin\varphi E_0^2}{4m\omega^2|\varepsilon_{\mathbf{k}}|\Omega}} \tag{2.120}$$

Eq (2.120) can be fully expanded as:

$$\langle\hat{\mathbf{M}}\rangle_{\mathrm{DC}} = \frac{Ne^3a\hbar v^2k\sin\varphi E_0^2}{4m\omega^2\sqrt{(\hbar\omega)^2+\left(\frac{2veE_0}{\omega}\right)^2}\sqrt{\frac{1}{4}\left(\sqrt{(\hbar\omega)^2+\left(\frac{2veE_0}{\omega}\right)^2}-\hbar\omega\right)^2+(\hbar vk)^2}} \tag{2.121}$$

Eq (2.121) physically describes the magnitude of the resultant DC magnetization vector that we expect to obtain by applying circularly polarized light to a sheet of graphene. As a sanity check, we can see that by setting the bandgap ε_g to zero, or in other words, setting $E_0 = 0$, the magnetization will vanish as well.

The term $k\sin\varphi$ in Eq (2.120) is the y-component of the wave vector $\mathbf{k}$. Since our Hamiltonian was constructed on the assumption that it is specifically for the regions very near the Dirac point K, the wave vector $\mathbf{k}$ has to be in that same region. For simplification, we have taken the Dirac point K itself as the value for $\mathbf{k}$. In other words,

$$\mathbf{k} = \mathbf{K} = \left(\frac{2\pi}{3a}, \frac{2\pi}{3\sqrt{3}a}\right), \tag{2.122}$$

$$k\sin\varphi = \frac{2\pi}{3\sqrt{3}a} \tag{2.123}$$

We can further simplify Eqs (2.120) and (2.121) with the above assumption:

$$\langle\hat{\mathbf{M}}\rangle_{\mathrm{DC}} = \frac{N\pi e^3\hbar v^2 E_0^2}{6\sqrt{3}\, m\omega^2|\varepsilon_{\mathbf{k}}|\Omega} \tag{2.124}$$

Expanding Eq (2.121) as a Taylor series in terms of E_0 as the variable, up to the sixth order, we will have:

$$\boxed{\langle\hat{\mathbf{M}}\rangle_{\mathrm{DC}} = \frac{Ne^3av}{8m\hbar\omega^3}E_0^2 - \frac{Ne^5av^3}{4m\hbar^3\omega^7}E_0^4 + \frac{Ne^7av^3(27a^2\omega^3 - 192\pi^2v^2)}{256\pi^2m\hbar^5\omega^{11}}E_0^6 + \dots} \tag{2.125}$$

The orders of the Taylor polynomial will be $2, 4, 6, \dots$, thus the DC magnetization is a function of E_0 in the form of $|\mathbf{E_p} \times \mathbf{E_p^*}|^N$ (where $N = 1, 2, 3, \dots$), as predicted by Majedi, A. Hamed and Lounis, Brahim [23]. We use the second order term in the Taylor expansion from Eq (2.125) to compare our result with other formulas derived for magnetization of graphene:

$$\langle\hat{\mathbf{M}}\rangle_{\mathrm{DC}} \simeq \frac{Ne^3av}{8m\hbar\omega^3}E_0^2 \tag{2.126}$$

Comparing Eq (2.126) with Pitaevskii's equation $\mathbf{M}_{\mathrm{DC}} = \gamma\mathbf{E} \times \mathbf{E}^*$, we obtain the optical gyration coefficient for our magnetization:

$$\gamma = \frac{iNe^3av}{16m\hbar\omega^3} \tag{2.127}$$

Furthermore, we observe that our result from Eq (2.126) is similar to the results obtained classically by Hertel [10], with the magnetization formula $\mathbf{M} = \frac{\langle n\rangle e^3}{2m^2\omega^3}$ where $\langle n\rangle$ is the time averaged electron density. Although the method here is completely different from that of Hertel, we see the same proportionalities of $\sim e^3$ and $\sim \omega^{-3}$. Comparing our result with Tokman *et al.* [33] shows even more similarities. Their expression for magnetization in graphene is:

$$m_z^{(0)} = \frac{e^3v^2}{2\pi c\hbar^2\omega^3}\frac{\left(\frac{2W_F}{\hbar}\right)^2 - 2\omega^2}{\left(\frac{2W_F}{\hbar}\right)^2 - \omega^2}\,\mathrm{Re}(i\tilde{E}_y\tilde{E}_x^*) \tag{2.128}$$

where W_F is the Fermi energy. Here we see the same proportionalities of $\sim e^3$, $\sim \omega^{-3}$ and also $\sim v^2$. However, our method of taking into account the band gap created in graphene due to the circularly polarized light results in no singularities in our expression for the magnetization, while the expression by Tokman *et al.* does contain a singularity in terms of the frequency ω.

Chapter 3

Numerical Results

In this section we will show our final results by looking at the equations derived in the previous section and plot them in regions of interest. The parameters used for the numerical calculations are given in Table 3.1.

Parameter	Symbol	Value
Graphene lattice constant	a_l	2.46 Å
Graphene nearest-neighbour atoms distance	a	1.42 Å
Orbital left shift	$\lvert\mathbf{R}_A\rvert$	0.71 Å
Orbital right shift	$\lvert\mathbf{R}_B\rvert$	0.71 Å
Fermi velocity in graphene	v_F	10^6 m/s
Graphene atomic density	N	$3.82 \times 10^{19}\,\mathrm{m}^{-2}$
Wave vector	$k \sin\varphi$	8.51549×10^9 m/s

Table 3.1: Parameters for numerical calculation

First, we will show the effect of the applied electric field strength and angular frequency on the dressed energy Ω which was given by Eq (2.8).

We take into account a realistic spectrum range for typical tunable lasers between the near ultraviolet (NUV) and near infrared (NIR) wavelengths. We note how the surface plot in Figure 3.1a looks entirely linear in the region of low electric field amplitudes and in a frequency range between $\omega = 1 \times 10^{15}$ s^{-1} to $\omega = 5 \times 10^{15}$ s^{-1}, corresponding to a wavelength range of $\lambda = 380$ nm to $\lambda = 1890$ nm. The energy $\hbar\omega$ is between 0.6582 eV and 1.3164 eV. It is clear that in this region, the energy is hardly dressed with any extra

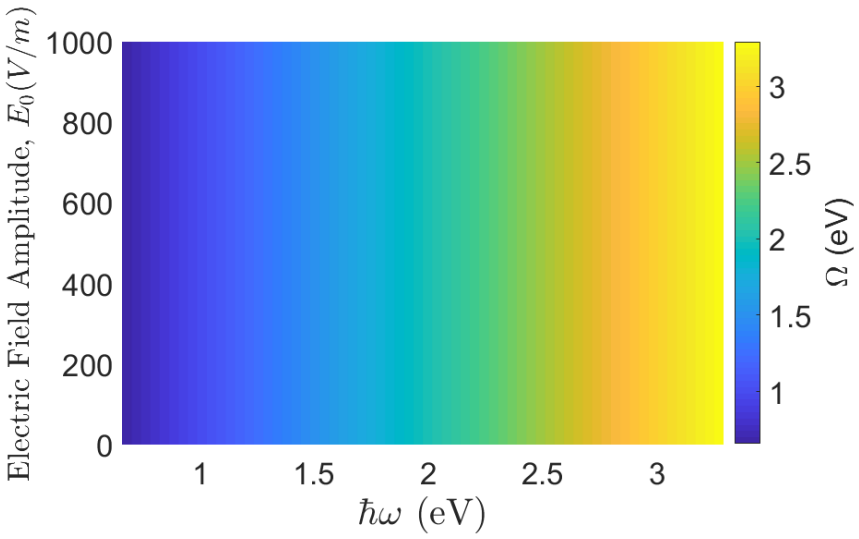

(a)

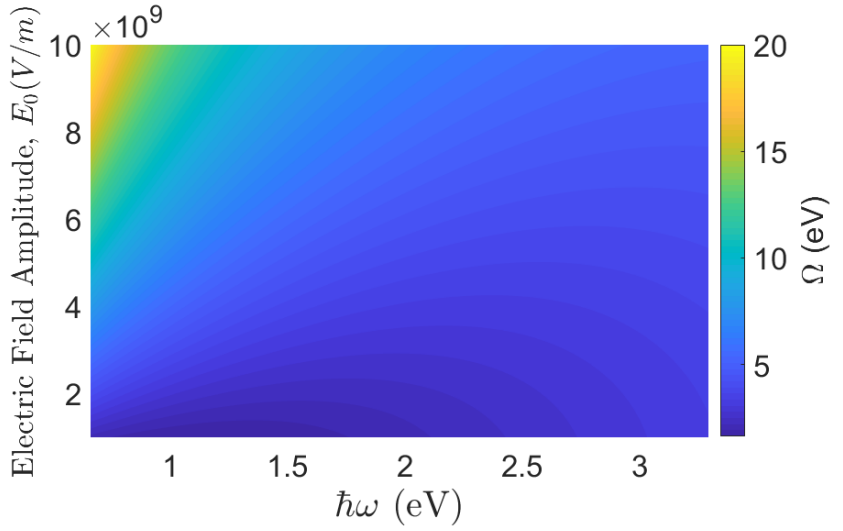

(b)

Figure 3.1: Surface plots for the dressed energy Ω with respect to field amplitude and energy, for high and low field amplitudes. Both figures are in the same frequency range of between $\omega = 1 \times 10^{15}$ s^{-1} to $\omega = 5 \times 10^{15}$ s^{-1} The electric amplitude range is (a) $E_0 = 0$ to $E_0 = 10^3$ V/m, (b) $E_0 = 10^9$ to $E_0 = 10^{10}$ V/m.

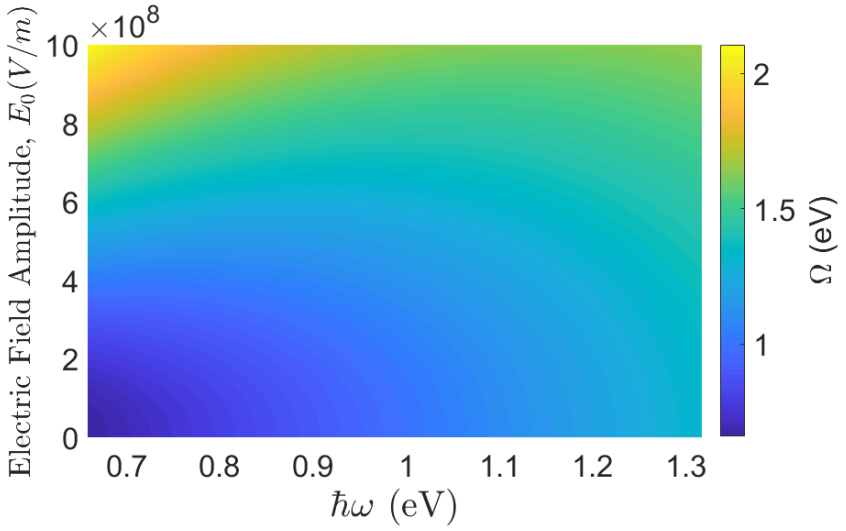

(a)

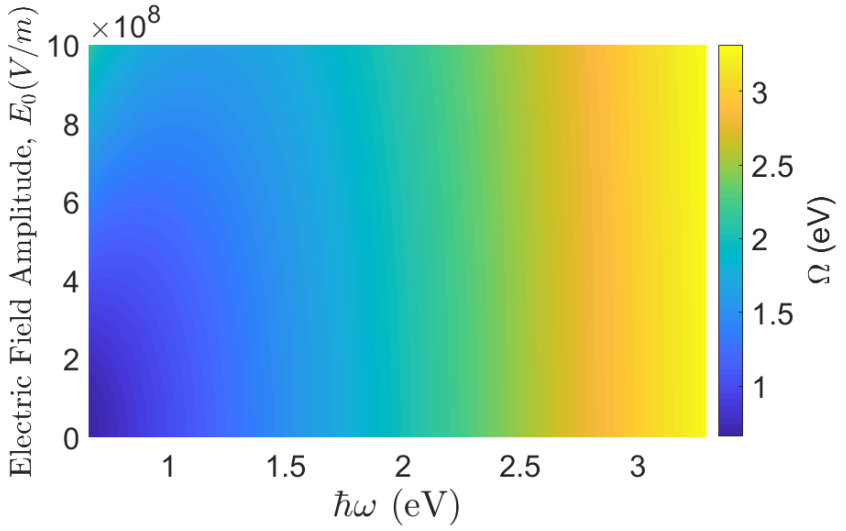

(b)

Figure 3.2: Surface plots for the dressed energy Ω with respect to field amplitude and energy, for high and low field amplitudes. Both figures are in the same electric field amplitude range of between $E_0 = 0$ V/m to $E_0 = 10^9$ V/m The electric amplitude range is (a) $\omega = 1 \times 10^{15}$ to $\omega = 2 \times 10^{15}$ s^{-1}, (b) $\omega = 1 \times 10^{15}$ to $\omega = 5 \times 10^{15}$ s^{-1}.

energy, and this is already clear from the equation. We can see a nearly seven-fold increase in the dressed energy when increasing the field amplitude from 10^3 to 10^9 V/m in Figure 3.1b. This corresponds to field intensities of $2.65\,\mathrm{W/cm^2}$ to $2.65 \times 10^{11}\,\mathrm{W/cm^2}$, easily attainable with lasers such as a Ti:Sapphire laser [8]. However, this maximum increase is mostly in the lowest range of frequencies in the selected range, meaning the lower original energy sees the most increase. What is more interesting is how we see a gradual shift in the surface plot gradient in Figure 3.2a to Figure 3.2b just by increasing the frequency range to a higher value. In Figure 3.2a, the dressed energy maximum is slightly higher than the original energy, but in Figure 3.2b, the dressed energy is almost the same. Much higher field amplitudes are required for significant dressed energies if the original energy is significantly high.

Finally, we will look at the magnetization formula we derived earlier and apply it to graphene as we plot the result.

Looking at Eq (2.124), one interesting observation that we also see numerically when graphing the magnetization plot is that there is an asymptote for the DC magnetization in terms of E_0 (choosing ω to be a constant.) Theoretically, we can determine this value by taking a limit:

$$\lim_{E_0 \to \infty} \frac{N\pi e^3 \hbar v^2 E_0^2}{6\sqrt{3}\, m\omega^2 |\varepsilon_{\mathbf{k}}| \Omega} = \frac{N\pi e\hbar}{12\sqrt{3}\, m} \tag{3.1}$$

This shows there is a saturation point for the DC magnetization which is directly related to very fundamental constants including the atomic number density of graphene, the graphene lattice constant, and electron charge. It is also inversely proportional to the mass of an electron. We have plotted this equation for frequency values of $\omega = 10^{15}$, 5×10^{15} and $10^{16}\ \mathrm{s^{-1}}$ with the saturation line at 1.071×10^{-4} A in Figure 3.3.

As can be seen from Figure 3.3b, the magnetization approaches this saturation value. There is also a maximum value for the magnetization for each frequency, but it is not shown in the plot as the range which the maximum can be viewed from the plot would be beyond experimentally viable intensities. We were unable to obtain analytical expressions for this maximum value, unlike the saturation point, but it is very simple to observe it with a graph and obtain them numerically.

Note that with an increase in angular frequency, this maximum magnetization value increases, but it also takes significantly more applied field intensity to for the magnetization to even rise above the saturation point. Compare the blue line in Figure 3.3a to the orange line. It is clear that for any realistic applications, frequencies above $10^{16}\ \mathrm{s^{-1}}$ are much less feasible because of the higher values of applied intensity required to get to the highest ranges of magnetization. As Figure 3.3b shows, very high intensity lasers are required for inducing

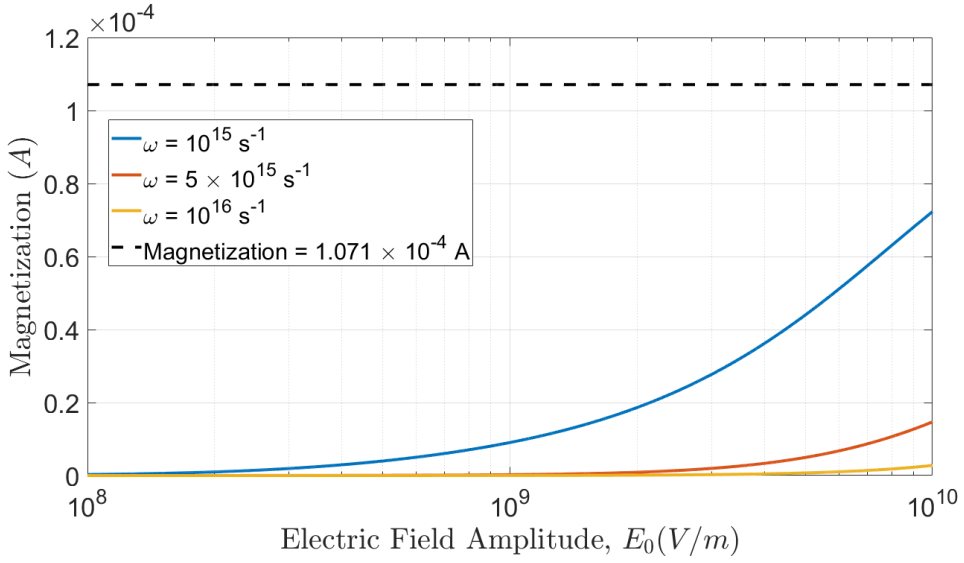

(a)

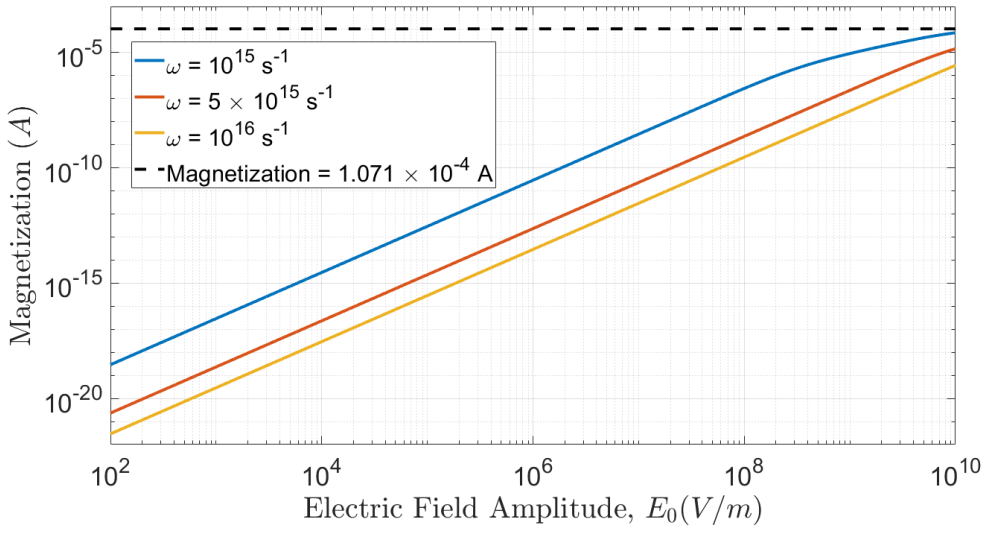

(b)

Figure 3.3: Magnetization plot with respect to field amplitude E_0. (a) Semi-log graph for the range of $E_0 = 10^8$ to 10^{10} V/m (intensity of 2.65×10^9 to $2.65 \times 10^{13}\,\mathrm{W/cm^2}$). (b) Log-log graph for the range of $E_0 = 10^2$ to 10^{10} V/m (intensity of 2.65×10^{-3} to $2.65 \times 10^{13}\,\mathrm{W/cm^2}$)

any significant magnetization. This was expected, as the induction of magnetization has been shown to be a nonlinear effect. In nonlinear optics, we generally employ ultrafast (femtoseconds) high intensity lasers for the experiments.

Figure 3.4 shows the magnetization for an experimentally applicable range of wavelengths of 800nm, 1000nm, 1650nm, 2000nm and 2500nm within a range of field intensities $I = 10^7$ to $I = 10^{13}$ W/cm^2.

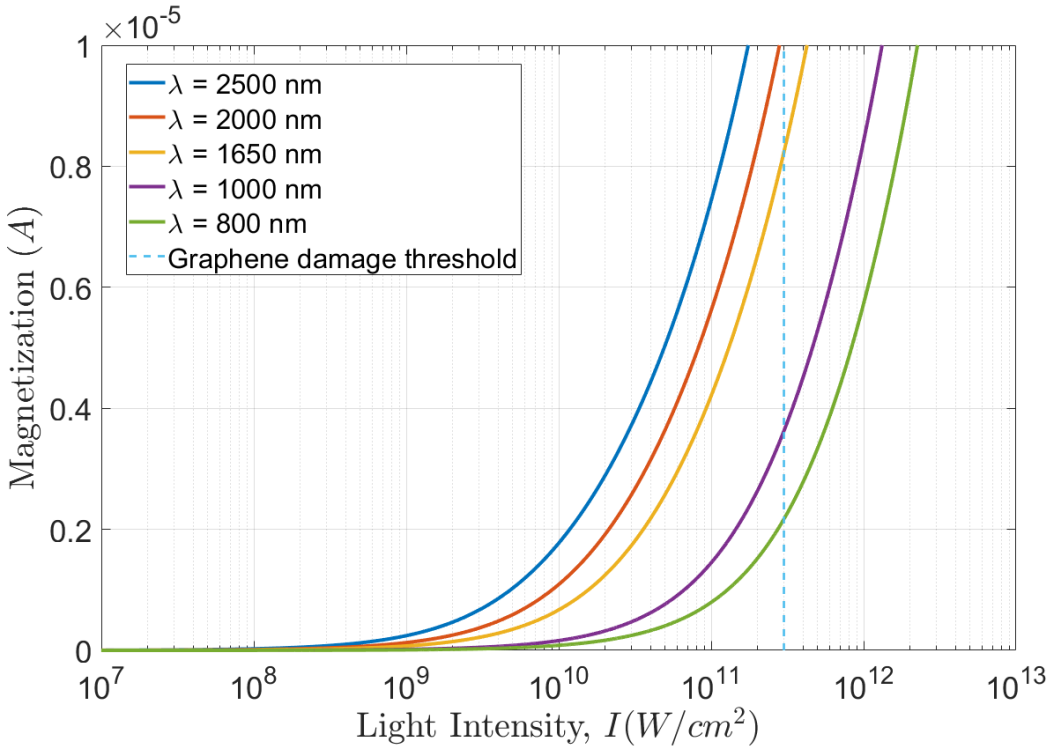

Figure 3.4: Semi-log graph of magnetization of graphene as a function of the light intensity I for the wavelength values 800nm, 1000nm, 1650nm, 2000nm and 2500nm.

Figure 3.5 shows the magnetization for the same range of wavelengths as Figure 3.4, but as a log-log graph in a wider range of intensities. Xing *et al.* estimate the intensity cutoff threshold for optical damage to graphene at 300 GW/cm^2 based on nonlinear optical measurements [35], which is what we have indicated in both of these figures by the blue dashed line. other research has shown that graphene has a single-shot damage threshold of $\sim 3 \times 10^{12}$ W/cm^2 with 50fs laser pulse [28].

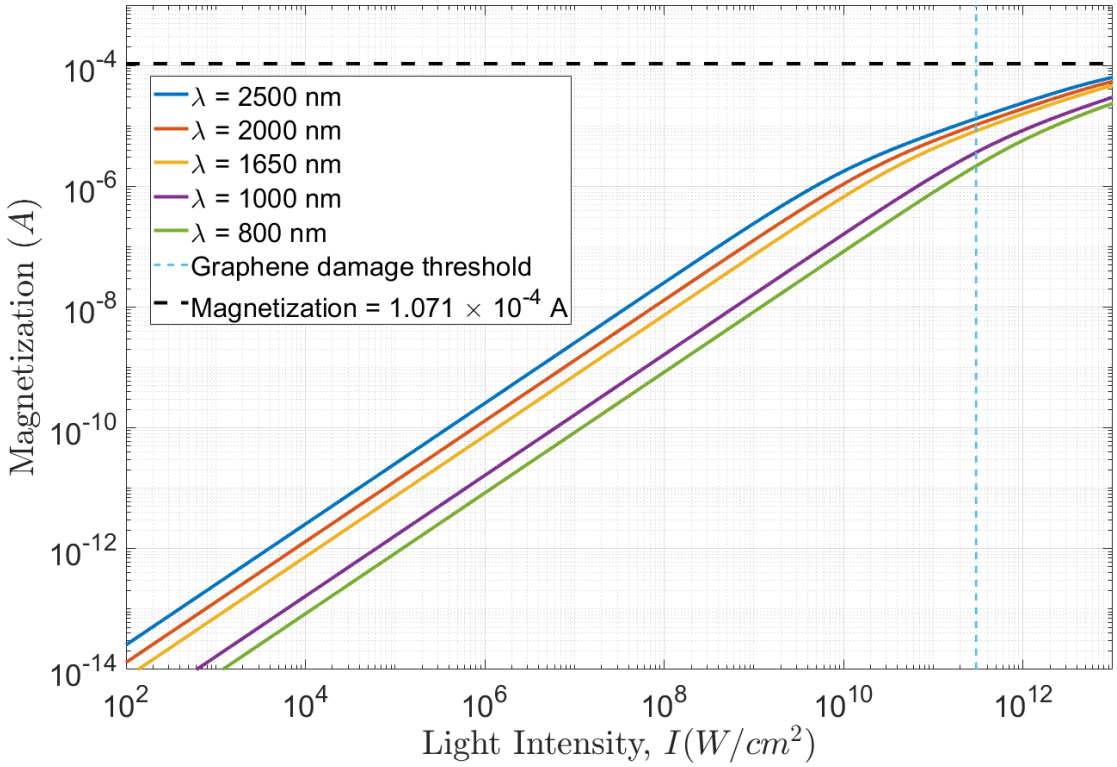

Figure 3.5: Log-log graph of magnetization of graphene for the wavelength values 800nm, 1000nm, 1650nm, 2000nm and 2500nm within a range of field intensities $I = 10^2$ to $I = 10^{13}\,\mathrm{W/cm^2}$. Note the increased value of magnetization with increasing wavelengths for the same intensity.

It is important to note that the units of magnetization here are given in Amperes (A) instead of A/m. Normally, the magnetic moment is given in units of $\mathrm{A} \cdot \mathrm{m}^2$ and the magnetization is defined as the magnetic moment divided by the volume of the material. In our case, the volume is replaced by the area of graphene, due to its 2D nature. We have confirmed this by dimensional analysis with Eq (2.120). It is interesting that in two dimensions, magnetization is difficult to distinguish from current itself in terms of units.

Finally, we can once again compare our results with the results of Tokman *et al.* [33] by comparing the magnetization values for a specific value of frequency and applied light intensity, ignoring their results for values of frequency which are near the singularity points as we do not have such singularities. In their paper, Tokman *et al.* use an applied circularly

polarized light with intensity of $10\,\mathrm{kW/cm^2}$ and vary the frequency. We compare the magnetization at one of their frequencies of $\hbar\omega = 100\,\mathrm{meV}$, which is equivalent to $\omega = 1.52 \times 10^{14}\,\mathrm{s^{-1}}$, with the magnetization from our own plot for the same frequency value and intensity. Tokman *et al.* predict a magnetization of $1 \times 10^{-10}\,\mathrm{G \cdot cm} = 7.85 \times 10^{-10}\mathrm{A}$, while we predict a magnetization of $3.09 \times 10^{-10}\mathrm{A}$. These values are on the same order and it further verifies that for any significant and detectable magnetization, a significantly high laser intensity is required.

Chapter 4

Conclusion

In conclusion, we fully derived the expression for the modified total wavefunction of graphene around the K point by solving the Schrödinger equation for the full Hamiltonian with the orbital functions $\Phi_1(\mathbf{r})$ and $\Phi_2(\mathbf{r})$ as the basis functions. We showed how the expression for the modified energy Ω and band gap ε_g appear from the procedure of solving for the total wavefunction.

We applied the resulting total wavefunction and the atomic orbital basis functions to the magnetization formula to obtain the final expression for the total magnetization induced by a circularly polarized light applied to a sheet of graphene. The total magnetization expression included both AC and DC terms, confirming that it is theoretically possible to obtain DC magnetization with this application of circularly polarized light. Importantly, this DC magnetization follows our expectation that this is a form of the Inverse Faraday Effect.

In the section on numerical results, we used the expressions from the analytical section to obtain several plots that showed the trends for both the modified energy amplitude and DC magnetization with respect to applied field amplitude E_0 and the applied field intensity I. We noted that there is a saturation magnetization with increasing intensities of light and noted that there are maximum values of magnetization for each wavelength (although not shown in the graphs.)

Since the predicted magnetization values even at relatively high applied intensities are very small, one possible method of detecting them is through SQUID (Superconducting QUantum Interference Device) magnetometry. This involves inducing a static magnetic field in graphene by an intense circularly polarized laser beam and direct magnetic field measurement by a mounted SQUID chip on the back of the graphene that is connected to

SQUID controller electronics. There are various measurement modes for SQUID such as VSM (Vibrating Sample Magnetometer), DC, etc., but we are not concerned with the mode at this point. One of the more widely used SQUID magnetometers, the MPMS (Magnetic Property Measuring System) has the sensitivity of $< 1 \times 10^{-8}$ emu, or equivalently, $< 1 \times 10^{-11} \mathrm{A} \cdot \mathrm{m}^2$ [4].

In a realistic scenario, we could have a 150fs applied laser pulse of wavelength 1650nm with a power of 10W concentrated in an area of 1µm × 1µm with a resulting intensity of $10^{13}\,\mathrm{W/m^2}$ or $10^{9}\,\mathrm{W/cm^2}$. Referring to the plot in Figure 3.5, the expected magnetization will be 7.3×10^{-8}A. This value must then be converted to magnetic moment by multiplying by the area of the graphene sheet. Assuming a graphene sheet of area 5mm × 5mm sits on a SiO_2/Si substrate (which also acts as a heat sink), the resulting magnetic moment will be $1.825 \times 10^{-12} \mathrm{A} \cdot \mathrm{m}^2$ which is lower than the sensitivity for this magnetometer. If we increase the power from 10W to 60W, the magnetization will be 4.19×10^{-7}A with a corresponding magnetic moment of $1.048 \times 10^{-11} \mathrm{A} \cdot \mathrm{m}^2$ which will be within the sensitivity limit of this SQUID model. The intensity of $6 \times 10^{9}\,\mathrm{W/cm^2}$ would be the absorbed intensity. However, this is without taking the absorption of graphene into consideration.

If we take into account the 2.3% absorption rate of graphene [14], the absorbed intensity for the above scenario would be $1.38 \times 10^{8}\,\mathrm{W/cm^2}$ which would give a magnetization of 1.012×10^{-8}A and a magnetic moment of $2.53 \times 10^{-13} \mathrm{A} \cdot \mathrm{m}^2$. This is outside the detectable range of the model we have mentioned. To be able to detect with the current MPMS model and the same sample size, the applied intensity would have to be increased to $2.8 \times 10^{11}\,\mathrm{W/cm^2}$ which is a significant increase in intensity, but still below the damage threshold of graphene.

Alternatively, it is possible to increase the area of the substrate as a way of increasing the magnetic moment for detection, but any higher values than already assumed could lead to problems with the measurement process of the SQUID itself [4]. Increasing the absorption rate of the graphene sheet is also another possibility [24], although it is most likely not sufficient by itself with the increased absorption rates that could be achieved. Higher wavelengths will also allows us to achieve higher magnetizations, but that is limited by the range of wavelength for lasers which is usually in the visible spectrum range.

It could also be possible to detect the magnetization more indirectly by passing linearly polarized light through the graphene sheet that has already been irradiated by circularly polarized light. If the rotation angle can be measured in that case, due to the similarity in concept of the Inverse Faraday Effect and the Faraday Effect, we should see a Faraday rotation directly proportional to the DC magnetization derived (although the expression for this rotation and its exact relation with the DC magnetization expression was beyond

the scope of this thesis.)

The importance of DC magnetization stressed throughout this thesis is that because of a lack of time-dependence, it opens up the possibility for ultrafast magnetization. In contrast to the bulk magneto-optical crystals, graphene combines high optical transmission with optomagnetic phenomena such as Faraday rotation in a two-dimensional platform making it attractive for integrated magneto-photonic devices and systems. From our results, we expect the possibility of creating electrically-tunable magneto-optical devices based on graphene structures and its combination with conventional photonic circuitry, i.e. integrated silicon photonics platform and silicon-based photonic band gap structures.

References

[1] M. Battiato, G. Barbalinardo, and P. M. Oppeneer. Quantum theory of the inverse faraday effect. *Phys. Rev. B*, 89:014413, Jan 2014.

[2] E. Beaurepaire, J.-C. Merle, A. Daunois, and J.-Y. Bigot. Ultrafast spin dynamics in ferromagnetic nickel. *Phys. Rev. Lett.*, 76:4250–4253, May 1996.

[3] Robert W. Boyd. *Nonlinear Optics, Third Edition*. Academic Press, Inc., USA, 3rd edition, 2008.

[4] M. Buchner, K. Höfler, B. Henne, V. Ney, and A. Ney. Tutorial: Basic principles, limits of detection, and pitfalls of highly sensitive squid magnetometry for nanomagnetism and spintronics. *Journal of Applied Physics*, 124(16):161101, 2018.

[5] A. A. Burkov. Topological semimetals. *Nature Materials*, 15(11):1145–1148, October 2016.

[6] Marc Currie, Joshua D. Caldwell, Francisco J. Bezares, Jeremy Robinson, Travis Anderson, Hayden Chun, and Marko Tadjer. Quantifying pulsed laser induced damage to graphene. *Applied Physics Letters*, 99(21):211909, 2011.

[7] N. P. Duong, T. Satoh, and M. Fiebig. Ultrafast manipulation of antiferromagnetism of nio. *Phys. Rev. Lett.*, 93:117402, Sep 2004.

[8] Rashid A. Ganeev. Chapter 1 - periodic nanoripples formation on the semiconductors possessing different bandgaps. In Rashid A. Ganeev, editor, *Nanostructured Nonlinear Optical Materials*, Advanced Nanomaterials, pages 1–38. Elsevier, 2018.

[9] V. N. Gridnev. Phenomenological theory for coherent magnon generation through impulsive stimulated raman scattering. *Phys. Rev. B*, 77:094426, Mar 2008.

[10] Riccardo Hertel. Theory of the inverse faraday effect in metals. *Journal of Magnetism and Magnetic Materials*, 303(1):L1 – L4, 2006.

[11] Riccardo Hertel and Manfred Fähnle. Macroscopic drift current in the inverse faraday effect. *Phys. Rev. B*, 91:020411, Jan 2015.

[12] Ganping Ju, A. V. Nurmikko, R. F. C. Farrow, R. F. Marks, M. J. Carey, and B. A. Gurney. Ultrafast optical modulation of an exchange biased ferromagnetic/antiferromagnetic bilayer. *Phys. Rev. B*, 58:R11857–R11860, Nov 1998.

[13] A. F. Kabychenkov. Magnetic phase transitions in a light wave. *Sov. Phys. JETP*, 73:672, October 1991.

[14] Mikhail I. Katsnelson. *Graphene: Carbon in Two Dimensions*. Cambridge University Press, 2012.

[15] A. V. Kimel, A. Kirilyuk, A. Tsvetkov, R. V. Pisarev, and Th. Rasing. Laser-induced ultrafast spin reorientation in the antiferromagnet tmfeo3. *Nature*, 429(6994):850–853, Jun 2004.

[16] A. V. Kimel, A. Kirilyuk, P. A. Usachev, R. V. Pisarev, A. M. Balbashov, and Th. Rasing. Ultrafast non-thermal control of magnetization by instantaneous photomagnetic pulses. *Nature*, 435(7042):655–657, Jun 2005.

[17] Andrei Kirilyuk, Alexey V. Kimel, and Theo Rasing. Ultrafast optical manipulation of magnetic order. *Rev. Mod. Phys.*, 82:2731–2784, Sep 2010.

[18] Mikhail A. Kozhaev, Alexander I. Chernov, Daria A. Sylgacheva, Alexander N. Shaposhnikov, Anatoly R. Prokopov, Vladimir N. Berzhansky, Anatoly K. Zvezdin, and Vladimir I. Belotelov. Giant peak of the inverse faraday effect in the band gap of magnetophotonic microcavity. *Scientific Reports*, 8(1):11435, Jul 2018.

[19] K. Kristinsson, O. V. Kibis, S. Morina, and I. A. Shelykh. Control of electronic transport in graphene by electromagnetic dressing. *Scientific Reports*, 6(1), February 2016.

[20] C-H. Lambert, S. Mangin, B. S. D. Ch. S. Varaprasad, Y. K. Takahashi, M. Hehn, M. Cinchetti, G. Malinowski, K. Hono, Y. Fainman, M. Aeschlimann, and E. E. Fullerton. All-optical control of ferromagnetic thin films and nanostructures. *Science*, 345(6202):1337–1340, 2014.

[21] Lev Davidovich Landau and E Lifshitz. On the theory of the dispersion of magnetic permeability in ferromagnetic bodies. *Phys. Z. Sowjet.*, 8:153, 1935.

[22] Jia-Ming Liu and I-Tan Lin. *Graphene Photonics*, pages i–ii. Cambridge University Press, 2018.

[23] A. Hamed Majedi and Brahim Lounis. Nonlinear optics of optomagnetics: Quantum and classical treatments. *Phys. Rev. B*, 102:214401, Dec 2020.

[24] N. Matthaiakakis, Xingzhao Yan, H. Mizuta, and M. D. B. Charlton. Tuneable strong optical absorption in a graphene-insulator-metal hybrid plasmonic device. *Scientific Reports*, 7(1), August 2017.

[25] P. S. Pershan. Nonlinear optical properties of solids: Energy considerations. *Phys. Rev.*, 130:919–929, May 1963.

[26] P. S. Pershan, J. P. van der Ziel, and L. D. Malmstrom. Theoretical discussion of the inverse faraday effect, raman scattering, and related phenomena. *Phys. Rev.*, 143:574–583, Mar 1966.

[27] Daria Popova, Andreas Bringer, and Stefan Blügel. Theory of the inverse faraday effect in view of ultrafast magnetization experiments. *Phys. Rev. B*, 84:214421, Dec 2011.

[28] Adam Roberts, Daniel Cormode, Collin Reynolds, Ty Newhouse-Illige, Brian J. LeRoy, and Arvinder S. Sandhu. Response of graphene to femtosecond high-intensity laser irradiation. *Applied Physics Letters*, 99(5):051912, 2011.

[29] R. Saito, G. Dresselhaus, and M.S. Dresselhaus. *Physical Properties of Carbon Nanotubes*. Imperial College Press, 1998.

[30] Yuen-Ron Shen. *The Principles of Nonlinear Optics*. Wiley Publishing, 2002.

[31] C. D. Stanciu, F. Hansteen, A. V. Kimel, A. Kirilyuk, A. Tsukamoto, A. Itoh, and Th. Rasing. All-optical magnetic recording with circularly polarized light. *Phys. Rev. Lett.*, 99:047601, Jul 2007.

[32] R. W. Teale and D. W. Temple. Photomagnetic anneal, a new magneto-optic effect, in si-doped yttrium iron garnet. *Phys. Rev. Lett.*, 19:904–905, Oct 1967.

[33] I. D. Tokman, Qianfan Chen, I. A. Shereshevsky, V. I. Pozdnyakova, Ivan Oladyshkin, Mikhail Tokman, and Alexey Belyanin. Inverse faraday effect in graphene and weyl semimetals. *Phys. Rev. B*, 101:174429, May 2020.

[34] J. P. van der Ziel, P. S. Pershan, and L. D. Malmstrom. Optically-induced magnetization resulting from the inverse faraday effect. *Phys. Rev. Lett.*, 15:190–193, Aug 1965.

[35] Guichuan Xing, Hongchen Guo, Xinhai Zhang, Tze Chien Sum, and Cheng Hon Alfred Huan. The physics of ultrafast saturable absorption in graphene. *Opt. Express*, 18(5):4564–4573, Mar 2010.

APPENDICES

Appendix A

Calculations with Linearly Polarized Light

In this appendix, we carry out similar calculations to the ones in section 2, except with a different vector potential (illustrated in Figure A.1):

$$\mathbf{A} = (A_0 \cos \omega t, 0) \tag{A.1}$$

Consequently, the Hamiltonians will be:

$$\begin{aligned}
\hat{\mathcal{H}}_0 &= -v\boldsymbol{\sigma} \cdot e\mathbf{A} \\
&= -ve(\sigma_x A_x + \sigma_y A_y) \\
&= -ve \left[\begin{pmatrix} 0 & 1 \\ 1 & 0 \end{pmatrix} (A_0 \cos \omega t) \right] \\
\hat{\mathcal{H}}_0 &= veA_0 \cos \omega t \begin{pmatrix} 0 & -1 \\ -1 & 0 \end{pmatrix}
\end{aligned} \tag{A.2}$$

$$\begin{aligned}
\hat{\mathcal{H}}_k &= v\boldsymbol{\sigma} \cdot \hbar\mathbf{k} \\
&= v\hbar(\sigma_x k_x + \sigma_y k_y) \\
&= v\hbar \left[\begin{pmatrix} 0 & 1 \\ 1 & 0 \end{pmatrix} k_x + \begin{pmatrix} 0 & -i \\ i & 0 \end{pmatrix} k_y \right] \\
&= v\hbar \begin{pmatrix} 0 & k_x - ik_y \\ k_x + ik_y & 0 \end{pmatrix} \\
\hat{\mathcal{H}}_k &= \begin{pmatrix} 0 & v\hbar(k_x - ik_y) \\ v\hbar(k_x + ik_y) & 0 \end{pmatrix}
\end{aligned} \tag{A.3}$$

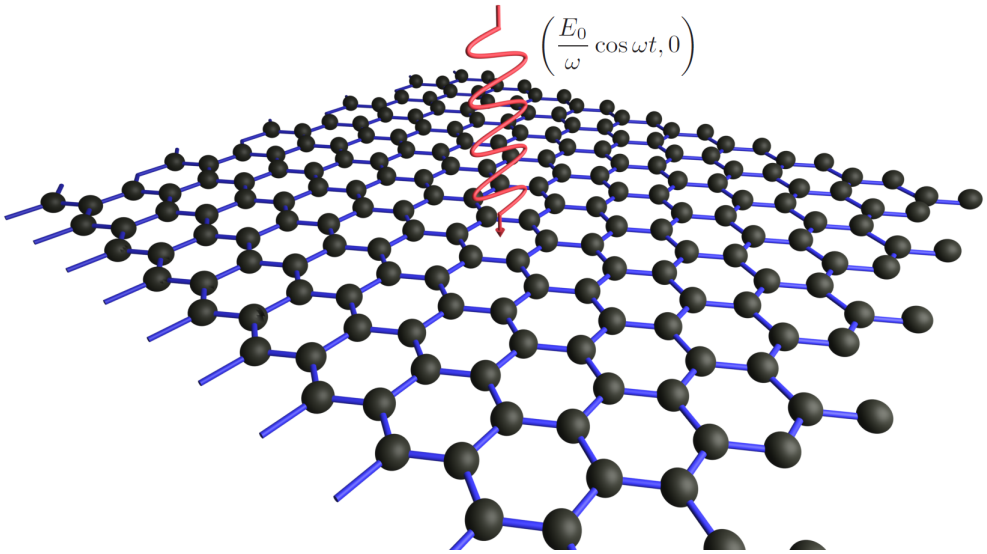

Figure A.1: Linearly polarized light applied to a sheet of graphene.

We assume the form of ψ_0 taken from the solution to Schrödinger's equation from $\hat{\mathcal{H}}_0$ to be:

$$\psi_0^{\pm} = \frac{1}{\sqrt{2}}\Big(\Phi_1'(\mathbf{r}) \pm \Phi_2'(\mathbf{r})\Big)e^{\pm i\frac{2veA_0}{\hbar\omega}\sin\omega t} \tag{A.4}$$

Similar to the previous section, we assume the solution to the Schrödinger equation for the total Hamiltonian to be:

$$\psi_{\mathbf{k}} = \xi^+ \begin{pmatrix} \psi_{01}^+ \\ \psi_{02}^+ \end{pmatrix} + \xi^- \begin{pmatrix} \psi_{01}^- \\ \psi_{02}^- \end{pmatrix} \tag{A.5}$$

Using the same algorithm for solving for the differential equations in ξ^+ and ξ^- by solving for ζ, δ^-, δ^+, Δ^-, Δ^+ with the new Hamiltonian, we will get the following expressions:

$$\begin{aligned} i\dot{\xi}^+ &= vk_x\xi^+ + ivk_y\xi^- e^{-i\frac{2veA_0}{\hbar\omega}\sin\omega t} \\ i\dot{\xi}^- &= -vk_x\xi^- - ivk_y\xi^+ e^{i\frac{2veA_0}{\hbar\omega}\sin\omega t} \end{aligned} \tag{A.6}$$

We use Floquet's theorem for $\xi^+(t)$ and $\xi^-(t)$:

$$\xi^{\pm}(t) = e^{-i\frac{\varepsilon_{\mathbf{k}}}{\hbar}t}\tilde{\xi}^{\pm}(t) \tag{A.7}$$

where

$$\tilde{\xi}^{\pm}(t) = \sum_{n=-\infty}^{\infty} c_n^{\pm} e^{in\omega t} \tag{A.8}$$

We also use the Jacobi-Anger expansion for the term that includes the exponential of the sine function [19]:

$$e^{iz\sin\theta} = \sum_{n=-\infty}^{\infty} J_n(z) e^{in\theta} \tag{A.9}$$

Where $J_n(z)$ is the nth order Bessel function. Before applying these expansions, we find the time derivatives of $\xi^{\pm}(t)$ according to these expansions:

$$\dot{\xi}^{+} = -i\frac{\varepsilon_{\mathbf{k}}}{\hbar} e^{-i\frac{\varepsilon_{\mathbf{k}}}{\hbar}t}\tilde{\xi}^{+} + e^{-i\frac{\varepsilon_{\mathbf{k}}}{\hbar}t}\dot{\tilde{\xi}}^{+} \tag{A.10}$$

$$\dot{\xi}^{-} = -i\frac{\varepsilon_{\mathbf{k}}}{\hbar} e^{-i\frac{\varepsilon_{\mathbf{k}}}{\hbar}t}\tilde{\xi}^{-} + e^{-i\frac{\varepsilon_{\mathbf{k}}}{\hbar}t}\dot{\tilde{\xi}}^{-} \tag{A.11}$$

We note that $\dot{\tilde{\xi}}^{\pm}$ can be written according to the expansion in equation (A.8):

$$\dot{\tilde{\xi}}^{\pm} = \sum_{n=-\infty}^{\infty} in\omega c_n^{\pm} e^{in\omega t} \tag{A.12}$$

We then applying expansions in equations (A.9), (A.10), (A.11) and (A.12) to the first equation in (A.6):

$$\begin{aligned} &i\left(-i\frac{\varepsilon_{\mathbf{k}}}{\hbar}e^{-i\frac{\varepsilon_{\mathbf{k}}}{\hbar}t}\sum_{n=-\infty}^{\infty} c_n^{+}e^{in\omega t} + e^{-i\frac{\varepsilon_{\mathbf{k}}}{\hbar}t}\sum_{n=-\infty}^{\infty} in\omega c_n^{+}e^{in\omega t}\right) = \\ &vk_x e^{-i\frac{\varepsilon_{\mathbf{k}}}{\hbar}t}\sum_{n=-\infty}^{\infty} c_n^{+}e^{in\omega t} + ivk_y e^{-i\frac{\varepsilon_{\mathbf{k}}}{\hbar}t}\sum_{n=-\infty}^{\infty} c_n^{-}e^{in\omega t}\sum_{m=-\infty}^{\infty} J_m\left(-\frac{2veA_0}{\hbar\omega}\right)e^{im\omega t} \end{aligned} \tag{A.13}$$

First we focus on the double summation in the final term on the right hand side of this equation to simplify it ($m'' = n + m$):

$$\sum_{n=-\infty}^{\infty} c_n^{-}e^{in\omega t}\sum_{m=-\infty}^{\infty} J_m\left(-\frac{2veA_0}{\hbar\omega}\right)e^{im\omega t} = \sum_{n,m=-\infty}^{\infty} e^{in\omega t}e^{im\omega t}c_n^{-}J_m\left(-\frac{2veA_0}{\hbar\omega}\right) \tag{A.14}$$

$$\sum_{n,m=-\infty}^{\infty} e^{in\omega t}e^{im\omega t}c_n^{-}J_m\left(\frac{2veA_0}{\hbar\omega}\right) = \sum_{m''=-\infty}^{\infty} e^{im''\omega t}\sum_{m=-\infty}^{\infty} c_{m''-m}^{-}J_m\left(-\frac{2veA_0}{\hbar\omega}\right) \tag{A.15}$$

Since m'' is a dummy index, we set $m'' = n$ so we will have:

$$\sum_{n=-\infty}^{\infty} e^{in\omega t} \sum_{m=-\infty}^{\infty} c_{n-m}^{-} J_m \left(-\frac{2veA_0}{\hbar\omega} \right) \tag{A.16}$$

Now using the result of equation (A.16) in equation (A.13):

$$\sum_{n=-\infty}^{\infty} e^{in\omega t} c_n^{+} \left[vk_x - \frac{\varepsilon_{\mathbf{k}}}{\hbar} - n\omega \right] + \sum_{n=-\infty}^{\infty} e^{in\omega t} \left[ivk_y \sum_{m=-\infty}^{\infty} c_{n-m}^{-} J_m \left(-\frac{2veA_0}{\hbar\omega} \right) \right] = 0 \tag{A.17}$$

Performing the same operation for the differential equation of $\xi^{-}(t)$ and applying the same results will give us the final equations:

$$\begin{aligned} \left(vk_x - \frac{\varepsilon_{\mathbf{k}}}{\hbar} - n\omega \right) c_n^{+} + ivk_y \sum_{m=-\infty}^{\infty} c_{n-m}^{-} J_m \left(-\frac{2veA_0}{\hbar\omega} \right) = 0 \\ \left(vk_x + \frac{\varepsilon_{\mathbf{k}}}{\hbar} + n\omega \right) c_n^{-} + ivk_y \sum_{m=-\infty}^{\infty} c_{n-m}^{+} J_m \left(\frac{2veA_0}{\hbar\omega} \right) = 0 \end{aligned} \tag{A.18}$$

For $n \neq 0$ and in the high-frequency field, equations (A.18) will become:

$$c_n^{\pm} \approx i \frac{vk_y}{n\omega} \sum_{m=-\infty}^{\infty} c_{n-m}^{\mp} J_m \left(\mp \frac{2veA_0}{\hbar\omega} \right) \tag{A.19}$$

Since $|c_n^{\pm}| \leq 1$ and $|J_m^{\pm}(z)| \leq 1$, all the terms except $c_0^{\pm}$ will vanish (i.e. $c_{n\neq 0}^{\pm} \approx 0$). Noting that $J_0(x) = J_0(-x)$, then equations (A.18) will simplify to:

$$\begin{aligned} \left(vk_x - \frac{\varepsilon_{\mathbf{k}}}{\hbar} \right) c_0^{+} + ivk_y c_0^{-} J_0 \left(\frac{2veA_0}{\hbar\omega} \right) = 0 \\ \left(vk_x + \frac{\varepsilon_{\mathbf{k}}}{\hbar} \right) c_0^{-} + ivk_y c_0^{+} J_0 \left(\frac{2veA_0}{\hbar\omega} \right) = 0 \end{aligned} \tag{A.20}$$

The determinant of this system of equations must be 0 to have consistent solutions:

$$\begin{aligned} 0 &= \left(vk_x - \frac{\varepsilon_{\mathbf{k}}}{\hbar} \right) \left(vk_x + \frac{\varepsilon_{\mathbf{k}}}{\hbar} \right) - \left(ivk_y J_0 \left(\frac{2veA_0}{\hbar\omega} \right) \right)^2 \\ &= (vk_x)^2 - \left(\frac{\varepsilon_{\mathbf{k}}}{\hbar} \right)^2 + (vk_y)^2 J_0^2 \left(\frac{2veA_0}{\hbar\omega} \right) \\ &= (vk\cos\varphi)^2 - \left(\frac{\varepsilon_{\mathbf{k}}}{\hbar} \right)^2 + (vk\sin\varphi)^2 J_0^2 \left(\frac{2veA_0}{\hbar\omega} \right) \\ 0 &= (\hbar vk\cos\varphi)^2 - \varepsilon_{\mathbf{k}}^2 + (\hbar vk\sin\varphi)^2 J_0^2 \left(\frac{2veA_0}{\hbar\omega} \right) \end{aligned} \tag{A.21}$$

Rearranging equation (A.21) in terms of $\varepsilon_{\mathbf{k}}$:

$$\varepsilon_{\mathbf{k}}^2 = (\hbar v k)^2 \left[\cos^2\varphi + \sin^2\varphi \left(\frac{2veA_0}{\hbar\omega}\right)\right] \tag{A.22}$$

Thus we get the final expression for $\varepsilon_{\mathbf{k}}$:

$$\varepsilon_{\mathbf{k}} = \pm\hbar v k f(\varphi) \tag{A.23}$$

where

$$f(\varphi) = \sqrt{\cos^2\varphi + J_0^2\left(\frac{2veA_0}{\hbar\omega}\right)\sin^2\varphi} \tag{A.24}$$

Now we need to find the $c_0^{\pm}$ terms themselves. We can easily deduce the normalization condition on these terms through equation (A.5). Like the previous section, the normalization condition will lead to the following equation:

$$\left|c_0^+\right|^2 + \left|c_0^-\right|^2 = 1 \tag{A.25}$$

Applying this normalization condition to equation (A.20):

$$\begin{aligned}
\left(vk_x - \frac{\varepsilon_{\mathbf{k}}}{\hbar}\right) c_0^+ &= -ivk_y c_0^- J_0\left(\frac{2veA_0}{\hbar\omega}\right) \\
\left(vk\cos\varphi - \frac{\varepsilon_{\mathbf{k}}}{\hbar}\right) c_0^+ &= -ivk\sin\varphi\, c_0^- J_0\left(\frac{2veA_0}{\hbar\omega}\right)
\end{aligned} \tag{A.26}$$

Taking the magnitude square of both sides:

$$\begin{aligned}
\left(vk\cos\varphi - \frac{\varepsilon_{\mathbf{k}}}{\hbar}\right)^2 \left|c_0^+\right|^2 &= (vk)^2\sin^2\varphi J_0^2\left(\frac{2veA_0}{\hbar\omega}\right)\left|c_0^-\right|^2 \\
\left(vk\cos\varphi - \frac{\varepsilon_{\mathbf{k}}}{\hbar}\right)^2 \left|c_0^+\right|^2 &= (vk)^2\sin^2\varphi J_0^2\left(\frac{2veA_0}{\hbar\omega}\right)\left(1 - \left|c_0^+\right|^2\right) \\
\left|c_0^+\right|^2 &= \frac{(vk)^2\sin^2\varphi J_0^2\left(\frac{2veA_0}{\hbar\omega}\right)}{\left(vk\cos\varphi - \frac{\varepsilon_{\mathbf{k}}}{\hbar}\right)^2 + (vk)^2\sin^2\varphi J_0^2\left(\frac{2veA_0}{\hbar\omega}\right)}
\end{aligned} \tag{A.27}$$

Simplifying further, noting that $\sin^2\varphi J_0^2\left(\frac{2veA_0}{\hbar\omega}\right) = f^2(\varphi) - \cos^2\varphi$ and also that $\frac{\varepsilon_{\mathbf{k}}}{\hbar} =$

$vkf(\varphi)$:

$$\begin{aligned}
\left|c_0^+\right|^2 &= \frac{(vk)^2\left(f^2(\varphi)-\cos^2\varphi\right)}{\left(vk\cos\varphi - vkf(\varphi)\right)^2 + (vk)^2\sin^2\varphi J_0^2\left(\frac{2veA_0}{\hbar\omega}\right)} \\
&= \frac{f^2(\varphi)-\cos^2\varphi}{\cos^2\varphi + f^2(\varphi) - 2\cos\varphi f(\varphi) + \sin^2\varphi J_0^2\left(\frac{2veA_0}{\hbar\omega}\right)} \\
&= \frac{f^2(\varphi)-\cos^2\varphi}{f^2(\varphi)+f^2(\varphi)-2\cos\varphi f(\varphi)} \\
&= \frac{f^2(\varphi)-\cos^2\varphi}{2f^2(\varphi)-2\cos\varphi f(\varphi)} \\
&= \frac{(f(\varphi)+\cos\varphi)(f(\varphi)-\cos\varphi)}{2f(\varphi)(f(\varphi)-\cos\varphi)} \\
&= \frac{\cos\varphi + f(\varphi)}{2f(\varphi)}
\end{aligned} \tag{A.28}$$

So we have:

$$c_0^+ = \pm\sqrt{\frac{\cos\varphi + f(\varphi)}{2f(\varphi)}} \tag{A.29}$$

We use the result from equation (A.29) in the second equation in (A.20):

$$\begin{aligned}
(vk\cos\varphi + vkf(\varphi))c_0^- &= -ivk\sin\varphi J_0\left(\frac{2veA_0}{\hbar\omega}\right)\left(\pm\sqrt{\frac{\cos\varphi+f(\varphi)}{2f(\varphi)}}\right) \\
(\cos\varphi + f(\varphi))c_0^- &= -i\sin\varphi J_0\left(\frac{2veA_0}{\hbar\omega}\right)\left(\pm\sqrt{\frac{\cos\varphi+f(\varphi)}{2f(\varphi)}}\right) \\
c_0^- &= \mp i\frac{\sin\varphi}{\cos\varphi+f(\varphi)}J_0\left(\frac{2veA_0}{\hbar\omega}\right)\sqrt{\frac{\cos\varphi+f(\varphi)}{2f(\varphi)}}
\end{aligned} \tag{A.30}$$

Now that we have found both c_0^+ and c_0^-, we can substitute them back into equation (A.5) to get the final dressed electron wavefunction $\psi_{\mathbf{k}}$:

$$\begin{aligned}
\psi_{\mathbf{k}} = \varphi_{\mathbf{k}}(\mathbf{r})e^{-i\frac{\varepsilon_{\mathbf{k}}}{\hbar}t}\sqrt{\frac{\cos\varphi+f(\varphi)}{4f(\varphi)}}\Bigg(&\pm\Big[\Phi_1(\mathbf{r})\pm\Phi_2(\mathbf{r})\Big]e^{\pm i\frac{2veA_0}{\hbar\omega}\sin\omega t} \\
&\mp i\frac{\sin\varphi}{\cos\varphi+f(\varphi)}J_0\left(\frac{2veA_0}{\hbar\omega}\right)\Big[\Phi_1(\mathbf{r})\mp\Phi_2(\mathbf{r})\Big]e^{\mp i\frac{2veA_0}{\hbar\omega}\sin\omega t}\Bigg)
\end{aligned} \tag{A.31}$$

This wavefunction can be used in the calculation of polarization with a similar method as before, by taking the expectation of the position operators to obtain an expression for the polarization vector which is equivalent to the form given by Boyd as $P = -Nex$ [3]. We have also looked at the possibility of finding the nonlinear refractive index of graphene using this method, but it is outside of the scope of this thesis.

Appendix B

Matlab Code

B.1 Integrals for the Expectation Value

All figure properties can also be manipulated from the command line. Here's an example:

```
a_0 = 1;                          % Bohr radius normalized to 1
a = 2.46e-10;                     % Graphene lattice constant
R_A = -a/(2*sqrt(3));             % Shift vector for atom A
R_B = a/(2*sqrt(3));              % Shift vector for atom B
norm = (1/(32*pi))*(6/a_0)^5;     % Normalization constant

I_11_z1 = @(x,y,z) norm * x.* z.^2 .* exp(-(6/a_0)*sqrt((x - R_A).^2 + ...
    + y.^2 + z.^2)); % Integrate the first of the two terms in I_11_z
I1 = integral3(I_11_z1,-inf,inf,-inf,inf,-inf,inf,'RelTol',1e-6);

I_11_z2 = @(x,y,z) norm * y.* z.^2 .* exp(-(6/a_0)*sqrt((x - R_B).^2 + ...
    y.^2 + z.^2));   % Integrate the second of the two terms in I_11_z
I2 = integral3(I_11_z2,-inf,inf,-inf,inf,-inf,inf,'RelTol',1e-6);

I_11_xy = @(x,y,z) norm * z.^3 .* exp(-(3/a_0)*sqrt((x - R_A).^2 + ...
    y.^2 + z.^2));   % Integrate I_11_x and I_11_y (they are equal)
I3 = integral3(I_11_xy,-inf,inf,-inf,inf,-inf,inf,'RelTol',1e-6);

I_12_z1 = @(x,y,z) norm * x.* z.^2 .* exp(-(3/a_0)*sqrt((x - R_A).^2 + ...
```

```
    y.^2 + z.^2)).* exp(-(3/a_0)*sqrt((x - R_B).^2 + y.^2 + z.^2));
I4 = integral3(I_12_z1,-inf,inf,-inf,inf,-inf,inf,'RelTol',1e-6);
% Integrate the first of the two terms in I_12_z

I_12_z2 = @(x,y,z) norm * y.* z.^2 .* exp(-(3/a_0)*sqrt((x - R_A).^2 + ...
    y.^2 + z.^2)).* exp(-(3/a_0)*sqrt((x - R_B).^2 + y.^2 + z.^2));
I5 = integral3(I_12_z1,-inf,inf,-inf,inf,-inf,inf,'RelTol',1e-6);
% Integrate the first of the two terms in I_12_z

I_12_xy = @(x,y,z) norm * z.^3 .* exp(-(3/a_0)*sqrt((x - R_A).^2 + ...
    y.^2 + z.^2)).* exp(-(3/a_0)*sqrt((x - R_B).^2 + y.^2 + z.^2));
I6 = integral3(I_12_xy,-inf,inf,-inf,inf,-inf,inf,'RelTol',1e-6);
% Integrate I_12_x and I_12_y (they are equal)
```

B.2 Code for Dressed Energy Plot

```
v = 1e6;                        % Fermi velocity in graphene (m/s)
charge = 1.60217662e-19;        % Electron charge (C)
hbar = 1.0545718e-34;           % Reduced Planck's constant (J.s)
joules_to_eV = 6.241509e18;     % Conversion factor from Joules to eV

E_0_start = 0;
E_0_end = 1e3;
w_start = 1e15;
w_end = 5e15;
E_0 = linspace(E_0_start,E_0_end,2000);
hw_space = joules_to_eV*hbar*linspace(w_start,w_end,2000);
[hw, E_0] = meshgrid(hw_space, E_0);
w = hw/((joules_to_eV*hbar));
Omega = sqrt((hw).^2 + (joules_to_eV*(2*v*charge.*E_0)./w).^2);

set(gca,'FontSize',30);
h = surf(hw, E_0, Omega);
set(h,'LineStyle','none')
c = colorbar('FontSize',30);
c.Label.String = '\Omega (eV)';
```

```
ax = gca;
ax.FontSize = 30;

xlabel('$\hbar \omega$ (eV)','interpreter','latex','FontSize',30);
ylabel('Electric Field Amplitude, $E_0 (V/m)$','interpreter','latex', ...
    'FontSize',30);
zlabel('$\Omega$ (eV)','FontSize',30);
view(2)
xlim([hw_space(1) hw_space(length(hw_space))]);
ylim([E_0_start E_0_end]);
```

B.3 Code for the Magnetization Plot

```
a = 2.46e-10;                       % Graphene lattice constant (m)
a2 = 1.42e-10;                      % Nearest-neighbour distance (m)
R_A = -a/(2*sqrt(3));               % Orbital shift (m)
v = 1e6;                            % Fermi velocity in graphene (m/s)
charge = 1.60217662e-19;            % Electron charge (C)
hbar = 1.0545718e-34;               % Reduced Planck's constant (J.s)
m = 9.10938356e-31;                 % Electron mass in kg
N = 3.82*10^19;                     % Graphene atomic density (m^-2)
k = 4*pi/(3*sqrt(3)*a2);            % Dirac point K (m^-1)
graphene_damage_cutoff = 3e11;      % Intensity W/cm^2
asymptote_value = N*pi*charge*hbar/(12*sqrt(3)*m);
format long

E_0 = logspace(2,10,100000);        % V/m
I = (E_0.^2/377)/(10^4);
w = [(2*pi*3*10^8)/(2500*10^-9) (2*pi*3*10^8)/(2000*10^-9) ...
    (2*pi*3*10^8)/(1650*10^-9) (2*pi*3*10^8)/(1000*10^-9) ...
    (2*pi*3*10^8)/(800*10^-9)];     % s^-1

Omega = zeros(length(w), length(E_0));
eg = zeros(length(w), length(E_0));
ek = zeros(length(w), length(E_0));
M_full = zeros(length(w), length(E_0));
```

```
asymptote_array = zeros(1, length(E_0));
asymptote_array(1,:) = asymptote_value;

for i=1:length(w)
    for j=1:length(E_0)
        Omega(i,j) = sqrt((hbar*w(i)).^2 + ((2*v*charge*E_0(j))./w(i)).^2);
        eg(i,j) = Omega(i,j) - hbar*w(i);
        ek(i,j) = sqrt((eg(i,j)/2).^2 + (hbar*v*k)^2);
        M_full(i,j) = (N*pi*charge^3*hbar*v^2*E_0(j).^2)./ ...
            (6*sqrt(3)*m*w(i).^2*ek(i,j).*Omega(i,j));
    end
end

loglog(I, M_full,'LineWidth',3)
hold on
semilogx([graphene_damage_cutoff graphene_damage_cutoff], ylim, ...
    'LineWidth',2,'LineStyle','--')
semilogx(I,asymptote_array,'LineWidth',3,'LineStyle','--','Color','black')
set(gca,'FontSize',26)
xlabel('Light Intensity, $I (W/cm^2)$','interpreter','latex','FontSize',30);
ylabel('Magnetization $(A)$','interpreter','latex','FontSize',30);
legend('\lambda = 2500 nm ','\lambda = 2000 nm ','\lambda = 1650 nm ', ...
    '\lambda = 1000 nm ','\lambda = 800 nm', ...
    'Graphene damage threshold', 'Magnetization = 1.071 \times 10^{-4} A');
xlim([10^2 10^13]);
ylim([10^-14 10^-3]);
grid on
hold off
```